Earth-Science Reviews 163 (2016) 297–322

Contents lists available at ScienceDirect

Earth-Science Reviews

journal homepage: www.elsevier.com/locate/earscirev

Indian winter monsoon: Present and past

A.P. Dimri [a,*], T. Yasunari [b], B.S. Kotlia [c], U.C. Mohanty [d], D.R. Sikka [e]

[a] School of Environmental Sciences, Jawaharlal Nehru University, New Delhi, India
[b] Research Institute for Humanity and Nature, Kyoto, Japan
[c] Centre of Advanced Study in Geology, Kumaun University, Nainital, Uttarakhand, India
[d] School of Earth Ocean and Climate Sciences, Indian Institute of Technology, Bhubaneswar, India
[e] Mausam Vihar, New Delhi, India

ARTICLE INFO

Article history:
Received 25 May 2016
Received in revised form 8 October 2016
Accepted 24 October 2016
Available online 29 October 2016

Keywords:
Indian winter monsoon
Western disturbances (WDs)
Subtropical westerly jet
Holocene
Little Ice Age
Monsoon breaks
Himalaya

ABSTRACT

The Indian subcontinent receives most of its annual precipitation due to Indian summer (June, July, August and September) monsoon. Southeastern coastal region of the India receives significant amount of precipitation due to the northeast monsoon (October and November). Over northern Indian region almost one-third of annual precipitation is received during winter (December, January and February) by eastward moving extratropical cyclone called 'western disturbances (WDs)' in Indian meteorological parlance. Various studies are conducted to understand the Indian summer and northeast monsoons. However, the dynamics and characterization of winter precipitation is not well understood except with reference to the western disturbances (WDs). In this study, wintertime dynamics associated with large-scale flows and WDs influencing winter precipitation is proposed and termed 'Indian winter monsoon'. In addition, winter precipitation – the Indian winter monsoon – is proposed as eastward traveling WDs embedded in the large-scale subtropical westerlies over the Indian sub-continent. During winter (December, January and February) upper level subtropical westerly jet moves southwards and passes over the Indian sub-continent and provides associated precipitation over the northern Indian region. With concurrent research and changing global context, increased understanding of the Indian winter monsoon is imperative. Equally important is the behavior of WDs showing different patterns in the Peninsular India and the Himalaya particularly during the Holocene. During the Little Ice Age (LIA), it appears that high frequency of El Niño events was responsible for drier conditions in the core monsoon zone but generated more monsoon "breaks" over the Himalaya and thus the climatic conditions in the core Indian summer monsoon area were generally opposite to those in the foothills of the Himalaya during the Holocene period. During this period, a higher frequency of El Niño events might have restricted transport of warm water to the North Atlantic Ocean and brought about a cooling of adjacent continents including Central Asia and this may have amplified the extent of snow over Asia during the winter, and may even have been accounted for early snow in the region at the expanse of reduction in the Indian summer monsoon strength. Thus, this study delineates the Indian winter monsoon at intraseasonal-sub seasonal-interannual-paleoclimate scale and provides comprehensive details on defining the Indian winter monsoon and makes an attempt to understand the WDs particularly from mid-Holocene onwards as well.

Contents

* Corresponding author at: School of Environmental Sciences, Jawaharlal Nehru University, New Delhi 110067, India.
E-mail address: apdimri@hotmail.com (A.P. Dimri).

http://dx.doi.org/10.1016/j.earscirev.2016.10.008
0012-8252/

1. Introduction

The Indian subcontinent is characterized by very unique geographic positioning. The north is surrounded by the mighty Himalaya and the south by oceans. Such situation along with many seasonal changes gives rise to different weather patterns over the Indian subcontinent. Indian summer monsoon (June, July, and August - JJA) (ISM) is researched and discussed along with its varying dimensions (Annamalai et al., 2007; KrishnaKumar et al., 1999, 2006; Turner et al., 2007). Tibetan high as well plays a significant role in defining the strength of it (Yasunari et al., 1991; Wu and Qian, 2003; Sato and Kimura, 2007). In case of northeast monsoon (NEM) Kripalani and Kumar (2004), Kumar et al. (2007) and Yadav (2012) have deliberated upon its dynamics comprehensively. In winter (December, January, and February - DJF) precipitation accumulation in the form of snow provides important feed to the north Indian rivers, glacier etc. during its melt season (Dai, 1990; Lang and Barros, 2004; Yadav et al., 2013; Dimri, 2014). This precipitation is mainly contributed by the extratropical cyclones associated subsurface low over Indian subcontinent and defined as western disturbances (WDs) (Dimri and Mohanty, 2009; Dimri et al., 2013). Though there are various researches available on ISM and NEM, very limited studies are available on the Indian winter monsoon (IWM) (Dimri, 2004, 2006, 2013a; Yadav et al., 2013). Only very few studies focused on its variability (Laat and Lelieveld, 2002; Dimri, 2013a, 2013b, 2013c; Yadav et al., 2013).

Further, many studies have defined dominant intraseasonal (ISO) modes varying at different time scales for ISM (Hartmann and Michelsen, 1989; Goswami and Mohan, 2001; Hoyos and Webster, 2007). Though the interannual variations (IAVs) in the IWM are in phase with El Niño Southern Oscillation (ENSO) forcings (Yadav et al., 2010; Dimri, 2013a, 2013c), very less is explained on its ISOs behavior (Dimri, 2014).

Since most of the Indian economy and agriculture is driven by ISM and may be due to its larger impact, most of the researches are focused on understanding the complexities associated with it. In case of IWM apart from its precipitation contributions over the northern Indian region, interactions with the northern Indian Himalayan topography and land use, paucity of observations, solid-liquid precipitation ratio and snow-covered land-surface interactions are some of the research questions that still need to be addressed/debated. With concurrent research and changing global context, studies of sub continental-scale circulation changes associated with IWM over northern India are imperative. In order to define the IWM, this paper elaborates on the potential role of sub-continental and global-scale circulation changes at intraseasonal-sub seasonal-interannual-paleoclimate scales associated with it. Such deliberation will provide new dimensions and definition to the understanding of IWM in Indian meteorological parlance which is missing thus so far. It is important to mention here that this synthesis will provide a distinct definition of IWM and differentiate it with NEM (which at times referred as Indian winter monsoon in Indian meteorological parlance as well). The following sections sequentially deliberate upon the important dynamics at various scales associated with the IWM.

2. Indian winter monsoon: present

2.1. Data and methodology

Precipitation fields from Asian Precipitation-Highly-Resolved Observational Data Integration Towards Evaluation of Water Resources (APHRODITE, Yatagai et al., 2012), Global Precipitation Climatology Project (GPCP, Adler et al., 2003), Global Precipitation Climatology Centre (GPCC, Rudolf et al., 2005) and Climate Research Unit (CRU, New et al., 2000) are used. Corresponding winter (December, January, February) precipitation over the western Himalaya (WH) from APHRODITE is shown in Fig. 1a. Idea of using multiple data sets is to assess the spatial variability of precipitation in different data products over the WH region. It is important because this region has paucity of observations and is having heterogeneous land use and variable topography. Wind, moisture, and geopotential fields are taken from the National Center of Environmental Predication/National Center for Atmospheric Research (NCEP/NCAR) at 2.5° horizontal resolution (Kanamitsu et al., 2002). Sea surface temperature (SST) at 1° horizontal resolution is considered from Hadley Center, UK (Hadley Centre, 2006). Long-term satellite estimates of outgoing longwave radiation (OLR) at 2.5° grid with monthly time intervals of the National Oceanic and Atmospheric Administration (NOAA), US are used to identify such seasonal and ground dependency (Liebmann and Smith, 1996). 28 winters (December 1979, January, February 1980 to December 2006, January, February 2007) data of height, wind, streamfunction, moisture flux etc. are considered to examine ISOs associated with the IWM.

Most of the algorithms used in preparing precipitation reanalysis generate 'synthetic' precipitation values which are at times away from the real observation particularly over the topographic regions. To remove this 'probable' bias of inadequate representation, a mask field of 10 mm/month precipitation threshold is forced. Also, precipitation, OLR, and reanalysis of daily anomalies are homogenized and deseasonalized. For each year first three harmonics of the annual cycle (about 120 days) are subtracted from the anomaly time series to homogenize it. Then to deseasonalize/detrend the time series, submonthly (7–25 days) perturbations were computed by applying a Lanczos filter (Duchon, 1979). In the WH, region from 30°N72°E to 37°N82°E (indicated by the box in Fig. 1a) was chosen to analyze winter precipitation and associated IAV and ISO. This region was chosen because it receives the highest winter precipitation and has variable topography. Fig. 1b shows the seasonal precipitation climatology based on APHRODITE. Winter precipitation is spatially distributed across and along WH topographic orientation. Precipitation maxima at ~34°N76°E and ~35°N72°E are observed. This climatology

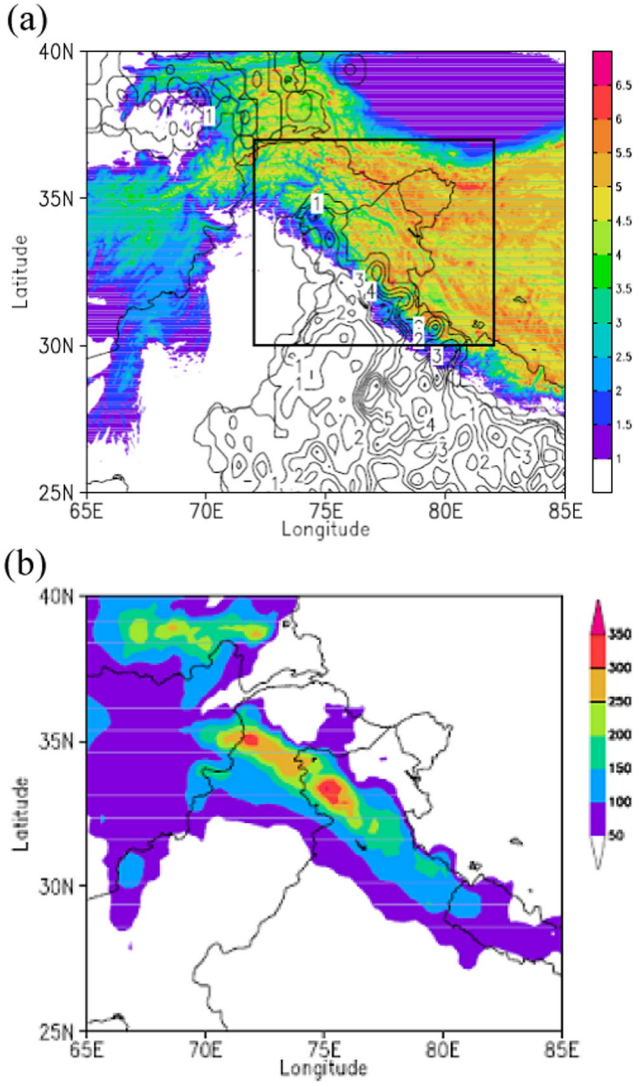

Fig. 1. (a) Topography (∗1e^{-3} m: shaded) and ratio of 0.05° grids for stations (%: contour) over the western Himalayas. The area of 30°N, 72°E to 37°N, 82°E is considered in the present study; (b) winter season precipitation climatology (mm/DJF) based on APHRODITE precipitation observed data reanalysis.

was compared with the other precipitation products (GPCP, GPCC, and CRU). Correlations as high as of >0.8 were recorded between APHRODITE and these reanalyzed data. Over WH, spatial precipitation patterns in all the four gridded data sets are similar. Of these four, APHRODITE is used for further analysis and discussion because it has the finest spatial resolution. It should be noted that over such region, some data may be 'synthetic' due to the various algorithms used while preparing the precipitation fields. Since this issue is beyond the scope of the present study, it is not deliberated here.

2.2. Winter storms/cold surges

The role of WDs in Indian weather was first presented by Pisharoty and Desai (1956). They explained dynamical synoptic situations of WDs in different seasons, and suggested that during wintertime, WDs are very similar to the Bjerknes cyclones of the Pacific and Atlantic (Fig. 2). Examining 10 years (1945–1955) precipitation records over the Indian subcontinent, Mooley (1957) systematically classified synoptic situations across the Himalayan region. In contrast to Pisharoty and Desai (1956), Mooley (1957) had pointed out that WDs are not similar to the extratropical depressions because they are not having well-marked cold or warm fronts at the surface or upper levels. This

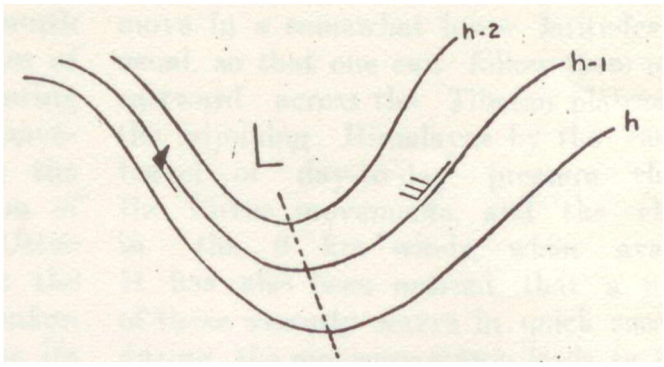

Fig. 2. An asymmetric upper-air trough with closer pecking in the rear (source: Mausam).

explanation added clarification to the presence of extratropical cyclones in mid-latitude westerlies. Indeed, Mooley (1957) showed that WDs are preceded by warm and moist air from southern latitudes, and succeeded by cold and dry air from northern latitudes. This was also the first extensive study linking the presence of WDs with the intensification of the ISM. This study examined various facets of WDs' structure, interactions with Himalayan topography, ISM, etc., but it did not provide a full description of the underlying dynamics. Riehl (1962) classified them as 'weak' extratropical disturbances originating in the Mediterranean, traveling with the narrow but intense jet stream flowing around the southern rim of the Indian Himalaya. Singh (1963) presented a comprehensive study of a WD, on 28–31 Dec. 1960, illustrating its vertical structure, evolution, decay, and associated jet stream movement. Singh's study showed that the vertical structure of WDs exhibits two synoptic components: an upper-level trough and a lower-level cyclonic circulation. This synopsis was supported by Ramaswamy (1966) as well. Datta and Gupta (1967) reported that the travel speed of WDs is of the order of 8 to 10° longitude/day (nearly equivalent to10–12 m/s) except during the formation and dissipation stages when the movement is comparatively slower, and has a life cycle duration of 3–4 days. Subsequently, the India Meteorological Department (IMD) published the first manual to guide forecast analysis at the synoptic scale (Rao and Srinivasan, 1969). Singh and Kumar (1977) confirmed Mooley's (1957) proposal that a well-organized upper tropospheric frontal layer in westerlies over a pre-existing surface low is essential for WD development, and that the organized upper-level front propagates eastward in association with an upper-air trough. Singh (1979) showed that WDs are strongly interlinked with mid-tropospheric westerly troughs. Growth of the upstream ridge is one of the key mechanisms to create a deep trough downstream (Singh et al., 1981). Singh (1971a, 1971b) illustrated the interaction of slower and more variant polar front jets located at 43°N with the subtropical westerly jet (SWJ). With the availability of satellite data, Rao and Moray (1971) provided an exhaustive analysis of cloud systems associated with WDs. While scrutinizing a large number of satellite pictures, they classified five cloud bands associated with WDs. Agnihotri and Singh (1982) illustrated three distinct types of cloud formations associated with extratropical depressions moving in northeastward from the Mediterranean. Kalsi and Halder (1992) linked cloud surges, due to integration of tropical and mid-latitude flows, with baroclinicity over the region. Together with many similar studies, a recent study by Puranik and Karekar (2009) showed the advancement of satellite technology while delineating the structure of WDs. They could depict mesoscale features of WDs based on information available in different bands of sensors. Ananthakrishnan and Keshavmurty (1973) revealed diagnostics based on kinetic energy budgets and energy conversions for large scale systems. They illustrated that kinetic energy generation due to meridional flow is consumed by zonal flow. Gupta and Mandal (1987) explained the behavior of the kinetic energy generation function during a WD. Agnihotri and Singh (1987) presented

the shortwave flux over the Indian subcontinent for the month of January only. They considered the effect of water vapor alone and illustrated that 60% of solar radiation gets absorbed within the surface to the 500 hPa level. Out of this, 58% is absorbed within the 1500 m height with rapid attenuation in solar radiation within this height. Mohanty et al. (1998, 1999) conducted studies using reanalyzed global data sets, which generated reasonably accurate large-scale circulation features and diagnostics associated with WDs over the data-sparse Himalaya. Further, Roy and Bhowmik (2005) analyzed the vertical thermodynamical structure of the atmosphere over Delhi during the passage of the WD based on model outputs. Their study revealed increased moisture at Delhi with the passage of the WD due to external advection of moisture over the station validating surface synoptic analysis. Dimri (2008), in brief, depicted various thermodynamical fluxes using model fields for a WD demonstrating the role of Himalayan orography in containing the vertical integrated moisture fluxes. Raju et al. (2011) have extensively delineated characteristic features associated with a WD for 19–21 January 1997. Their results showed that strong flux convergence and adiabatic production of kinetic energy takes place during the passage of a WD over northern India. The meridional component of the kinetic energy was found to contribute to the generation, whereas the zonal component of the kinetic energy contributes to the destruction in adiabatic generation of kinetic energy along the track of the WD. In numerical modeling progression, Rao and Rao (1971) provided the first simple theoretical and synoptic model basis for WDs. Ramanathan and Saha (1972) applied a primitive equation barotropic model at 500 hPa to predict the movement of WDs and initiated a process of employing numerical modeling efforts for forecasting purposes while documenting initial and boundary problems. Chitlangia (1976) employed a moving coordinate system to study the mean structure of a WD. Dash and Chakrapani (1989) gave a comprehensive analysis of a simulated WD using a global spectral model. Azadi et al. (2001) showed the effect of various combinations of planetary boundary layer and convection parameterization schemes while simulating precipitation associated with a WD based on a mesoscale model (MM5V3). Das et al. (2003) describes the increased importance and status of mesoscale modeling for mountain weather forecasting in the Himalaya. Dimri (2004) presented the interaction of topography and WDs while simulating a WD with a mesoscale model (MM5V3). This study revealed the potential of mesoscale models for accurate real-time prediction of WDs. Das (2005) and Hatwar et al. (2005) provided comprehensive details on prediction abilities of a mesoscale model (MM5V3) for a WD. The utility of real-time prediction of a WD in defining natural hazard (avalanche) forecasting was documented in Srinivasan et al. (2005). These studies have provided rationale for real-time prediction of WDs. Azadi et al. (2005) while simulating a number of WDs with the MM5 modeling system, concluded that model simulated zonal winds are generally weaker and underestimated in the upper trough at 500 hPa or aloft and even at lower levels. With a number of experimental model set-ups (different combinations of topography, no topography, planetary boundary layer schemes, and convective parameterization schemes) Dimri et al. (2004) showed model physics and dynamics in precipitation forming mechanisms associated with WDs. Semwal and Giri (2007) used a mesoscale model (ARPS) forced with global spectral model (T80) outputs. This study provided realistic configuration of real-time prediction. Dimri and Mohanty (2009) illustrated growing errors in time integration while simulating WDs using MM5. These studies suggest that models have systematic biases. Hara et al. (2004) described the mechanism of WDs over the Himalaya while Semwal and Dimri (2012) used different initial and boundary conditions within the ARPS modeling framework for best prediction suite. Three-dimensional variation assimilation techniques using the MODIS thermodynamical profile is presented in Rakesh et al. (2009), and Dasgupta et al. (2012) used surface observations to simulate a WD using the MM5 modeling system. Both of these studies show remarkable improvements on model efforts on WDs simulations and results. Dimri and Niyogi (2012) presented the precipitation mechanism associated with interaction of topography with the WD (Fig. 3). Thomas et al. (2013) showed the role of land use while studying WDs.

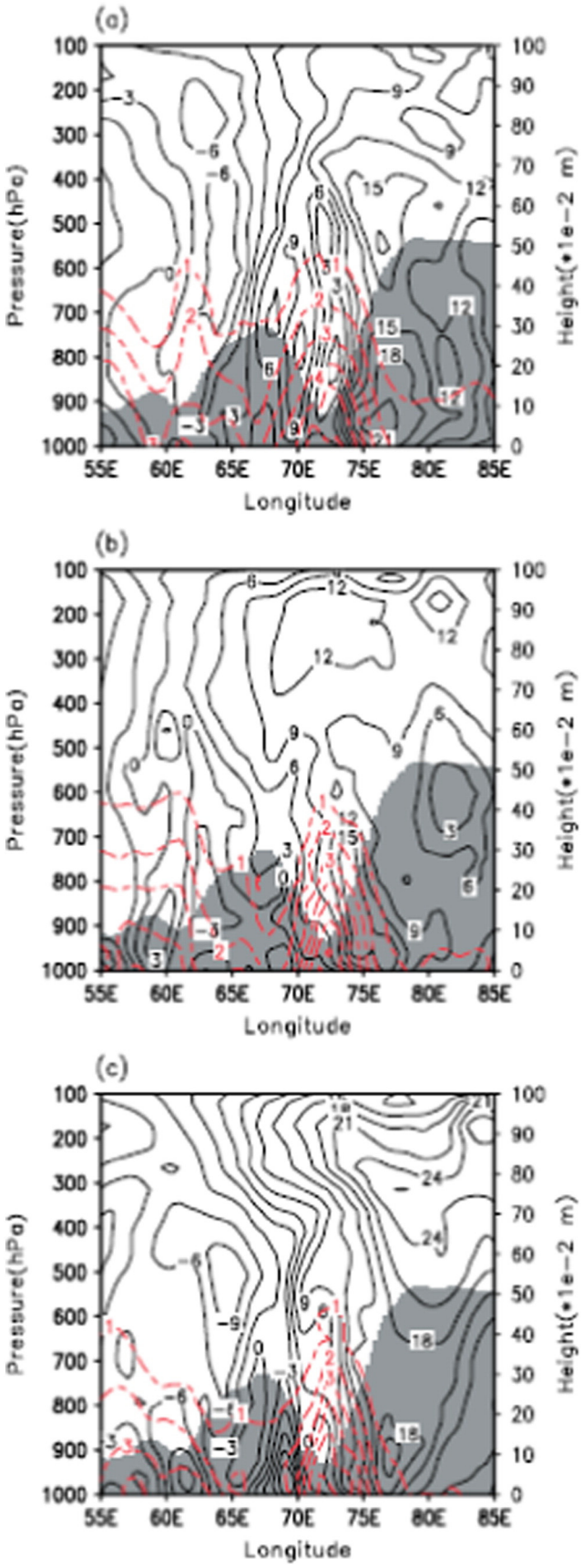

2.3. Intraseasonal oscillation (ISO)

Here robust features of ISOs of the IWM and associated atmospheric circulation patterns are discussed. 28 years WH daily precipitation (hereafter WHDP) (bar), corresponding pentad climatology (black curve with open circles) and 7–25-day filtered precipitation (red curve with open circles) is shown in Fig. 4a. ISO at sub-monthly timescales with active and break peaks is seen. To define it, active (break) peak phases are considered which exceeded above (below) the 28-winter climatological 0.5 standard deviation in the 7–25-day WHDP anomalies. On doing so 140 active and 119 break peak phases are identified. To investigate temporal relationship of WHDP variability, circulation fields, OLR composites and daily time lag composites were used.

2.3.1. Results and discussion

2.3.1.1. Intraseasonal variability in WHDP. Using Fast Fourier Transform (FFT), dominant mode of ISO in the WHDP during the 28 winters was seen. WHDP (the first three harmonics of the annual cycle were removed) is detrended and masked from 15 Nov. to 15 Mar. (120 days) (Dimri, 2013a, 2013b, 2013c). Fig. 4b and c shows the FFT spectrum for WHDP for 28 winters. A pronounced periodic ~16-day peak with a 95% statistical significance appears (Fig. 4b). Corresponding Fig. 4c presents 28 years' power spectrum of interannual variation (IAV) of the WHDP showing approximately a 16-day period scale in each year. This corresponds closely with the ensemble spectrum (Fig. 4b) at sub-monthly-scale. Hence analysis of ISO mode of ~7–25 days periodicity in WHDP is proposed.

2.3.1.2. Atmospheric circulation and convection fields. Sub-monthly scale space-time structure of the atmospheric circulation and convection in composites of active and break is investigated. Total 140 active and 119 break peak phases are chosen out of 28 years climatology. Daily lag composite of vertically integrated moisture flux and divergence from day −8 to day +8 based on the 7–25-day precipitation variation over the WH is presented in Fig. 5a. Day 0 corresponds to active precipitation peak phases and day −8 and day +8 corresponds to break peak phases. This cycle corresponds to a composite variation of 16 days. Peak break phase is characterized by divergence over the WH with moisture exiting out of the region. On day −6, convergence builds up over the Arabian Sea near the Gujarat coast with fluxes still exiting out from the WH. On subsequent day −4, subtle changes in flux direction with shift in convergence zone towards the Himalaya are observed. Crucial flow transfer starts by this time with two breakaway streams. First one flows into the WH and second moving farther out from the eastern Himalaya. During precipitation peaks in the active phases, well-defined moisture influx with well-defined convergence zone over the Himalaya sets in. This characteristic weakens by day +2 with increased outflow and divergence over the Himalaya. Such situation dominates and strengthens during the following days.

Daily lag composites of 500 hPa streamfunction and wind from day −8 to day +8 based on 7–25-day precipitation variation over the WH are investigated to establish the character of dynamical atmosphere (Fig. 6). An anomalous higher streamfunction, corresponding to anticyclonic circulation builds up over the western part of the WH on day −8. This moves eastwards on subsequent days. With this, on day −4, anomalous cyclonic circulation characterized by lower streamfunction

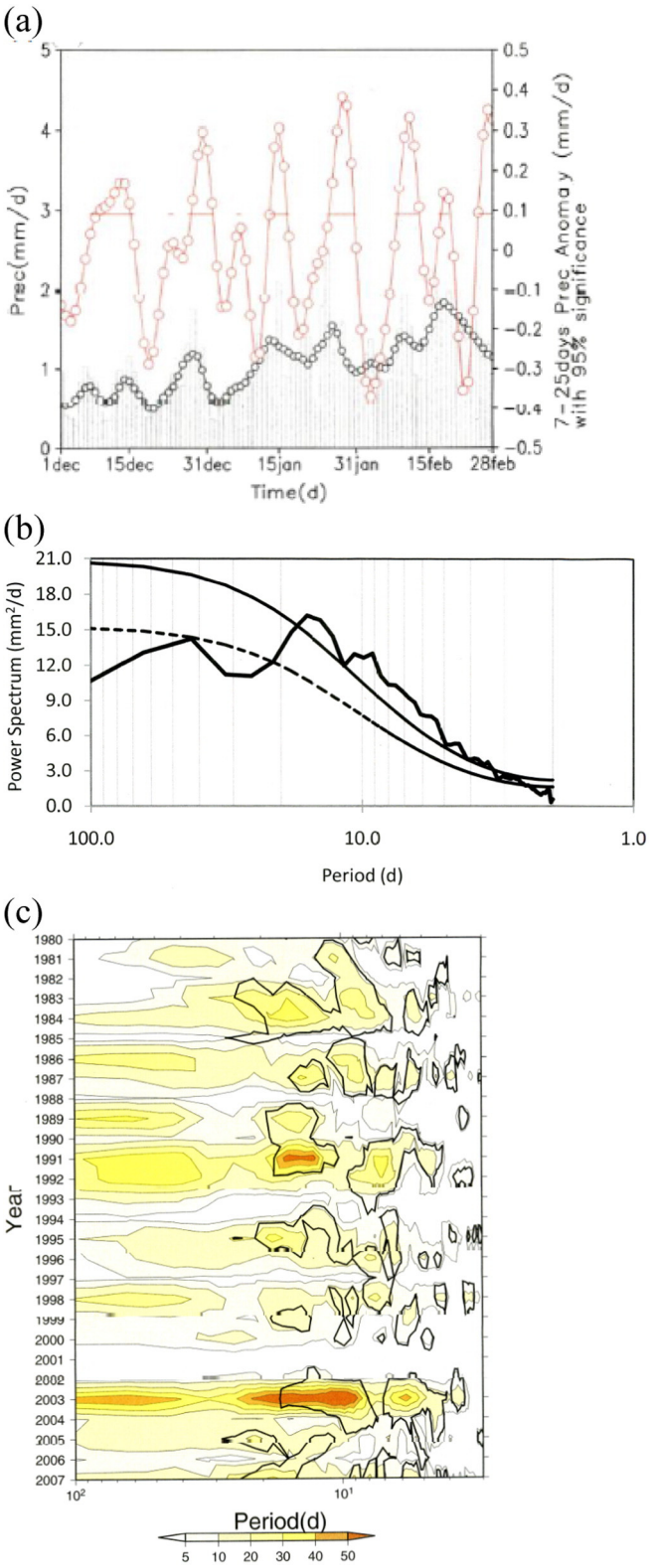

Fig. 4. (a) Based on 28 years (Dec. 1979, Jan., Feb. 1980 to Dec. 2006, Jan., Feb. 2007) of data, time-series of WHDP climatology (bar; left axis), pentad precipitation climatology (black line with open circles; left axis), and 7–25-day filtered precipitation anomaly (red line with open circles; right axis). The line of 95% significance is also shown and the period above this corresponds to climatological active phases. (b) The 28-winter (DJF) ensemble spectrum of the WHDP time series from 15 Nov. to 15 Mar. (120 days). A red noise spectrum (dashed curve) and its 95% level of significance (solid curve) are also shown. (c) Interannual variation in the WHDP spectrum from 1980 to 2007. The thick black solid line shows the 95% level of significance. (For interpretation of the references to color in this figure legend, the reader is referred to the web version of this article.)

Fig. 3. Longitude-pressure cross section vertical distribution at 34°N latitude of model-simulated meridional wind (m/s) (continuous black contour) and air specific humidity ($*1e^{-3}$) (broken red contour) at 0000 UTC during active WD. (a) 21 Jan. 1999 (b) 22 Jan. 1999 (c) 23 Jan. 1999. (Left-hand side vertical axis corresponds to the pressure distribution and right-hand side vertical axis corresponds to the topography $*1e^{-2}$ m). (For interpretation of the references to color in this figure legend, the reader is referred to the web version of this article.)

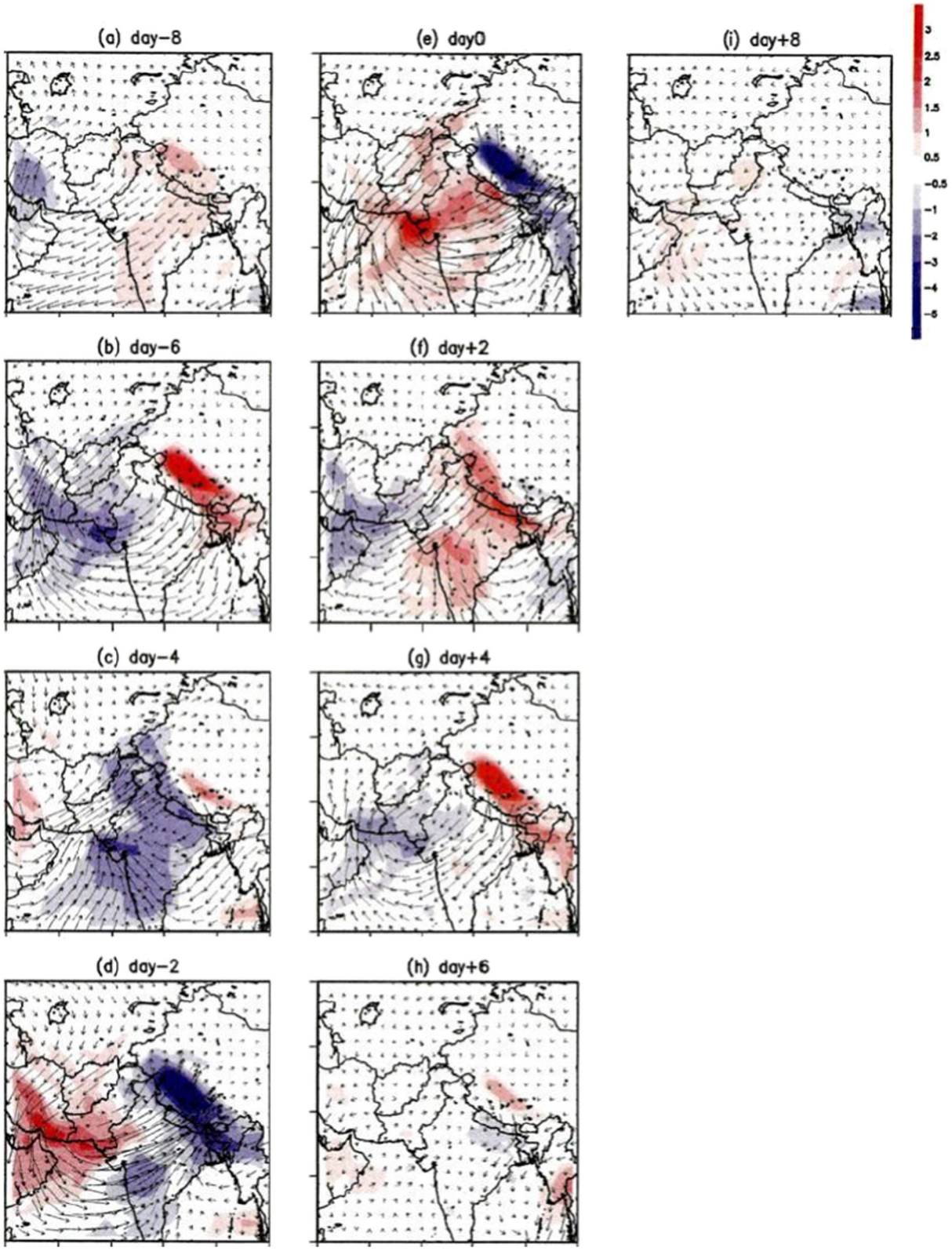

Fig. 5. Composite of vertical integrated moisture flux (vector, 40 kg/m/s) and divergence (shaded, $*1e^5$/s) based on 7–25-day filtered values of specific humidity and wind anomalous fields from day −8 to day +8 based on WHDP. Day 0 corresponds to the active peak of 7–25-day WHDP variation. Values above 95% statistically significant are plotted with shade.

values develops over Saudi Arabia. Significant winds succeeding (preceding) the anomalous anticyclonic (cyclonic) circulation are seen. This situation of anomalous cyclonic circulation intensified and moved eastward over the Afghanistan and Pakistan region by day −2. Such situation as well is associated with strong winds. On peak phase, day 0, intense wind, located over the WH and adjoining Pakistan region dominates. It is interesting to note that the center of anomalous cyclonic circulation over and near the WH persists for at least 04 day, from day

−2 to day +2. Such positioning provides conducive situation for southwesterly moisture influx from the Arabian Sea during active peak phases. This dominance in association with WDs' life cycle defines the reasoning of higher precipitation in active phases. The Himalayan topography stagnates and/or changes the direction of the southwesterly flow and the significant winds and thus weakens their strength. At

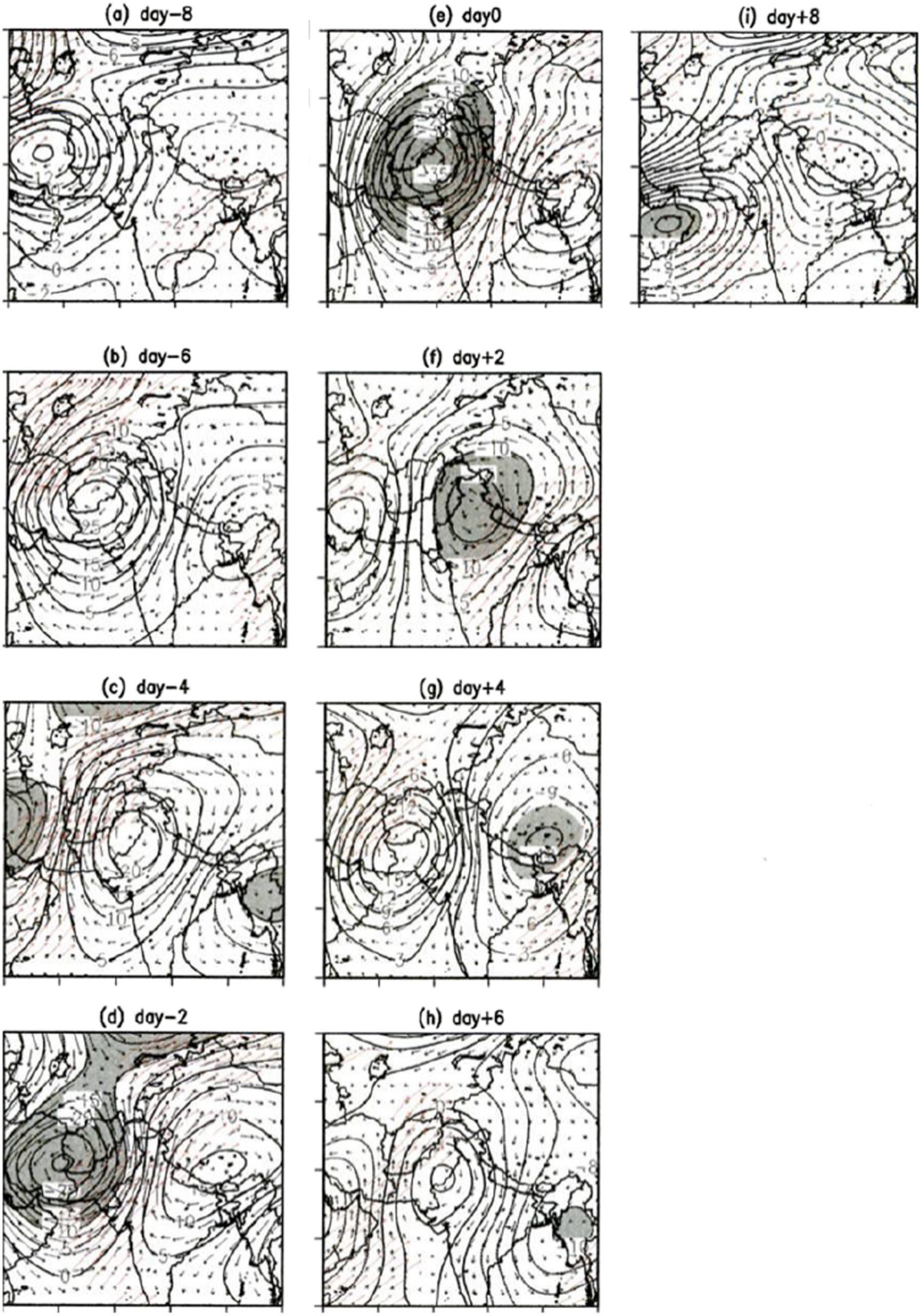

Fig. 6. Composite of 7–25-day filtered 500 hPa streamfunction ($*1e^{-6}$ m^2/s) and wind (m/s) anomalies from day −8 to day +8 based on WHDP. Day 0 corresponds to the active peak of 7–25-day WHDP variation. The contour interval for streamfunction is $5 * 1e^{-6}$ m^2/s, and the 95% statistically significant streamfunction is shaded. The strength of the wind vector is 15 m/s, and the 95% statistically significant wind is plotted with red color. (For interpretation of the references to color in this figure legend, the reader is referred to the web version of this article.)

upper troposphere (200 hPa-data not shown) similar structure of mid-troposphere dominates except that at this level, larger and elongated significant area with significant southwesterly winds preceding the system persists. This vertical distribution of deep cyclonic circulation extends from mid- to upper troposphere during the peak active phase. Anomalous anticyclonic and cyclonic circulations persist in cascading manner in the upper troposphere which on subsequent days decay and so on. The upper tropospheric anomalous cyclonic circulation persists longer as compared to the mid-tropospheric one.

Further OLR distribution from day −8 to day +8 based on the 7–25-day precipitation along with a similar distribution of 500 hPa stream function and wind as shown in Fig. 6 (for better assessment) is

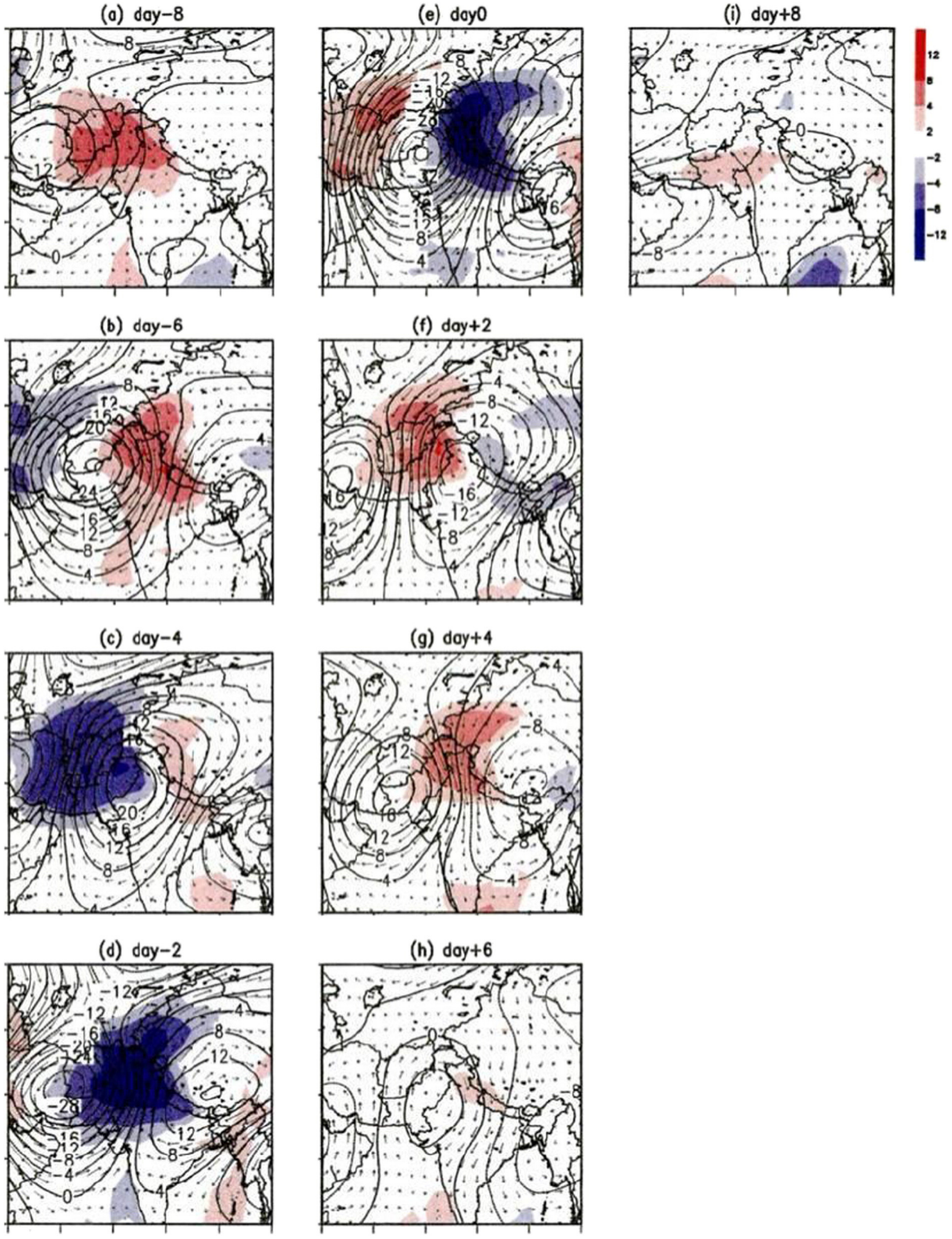

Fig. 7. Composite of 7–25-day filtered OLR (W/m^2; shade), 500-hPa streamfunction ($*1e^{-6}$ m^2/s), and wind (m/s) anomalies from day −8 to day +8 based on WHDP. Day 0 corresponds to the active peak of 7–25-day WHDP variation. The contour interval for streamfunction is $4 * 1e^{-6}$ m^2/s. The strength of the wind vector is 5 m/s.

illustrated in Fig. 7. Increased and faster advancement of the anomalous cyclonic circulation due to suppressed convection dominates over the Himalayan region. This deepens by day −4. Further build-up of convection leads to more localized precipitation over the WH. Increased (suppressed) convection ahead (rear) of the anomalous cyclonic circulation is seen. Active peak displays strongest convection ahead of anomalous cyclonic circulation on day 0. Here as well similar situation occurring in a cascading manner is seen which corresponds to chain of anomalous cyclonic circulations, followed by another anomalous anticyclonic circulation, and so on.

To understand the periodic occurrences of alternating anomalous anticyclonic and cyclonic circulations and its association with associated precipitation, Fig. 8 presents time-lag composites based on 7–25-day active peak phases. It shows evolution of cyclonic systems which is in correspondence with the life cycle of the WDs. This conformity of WDs as a "family," with one following the other in a symmetric wave which peaks at day 0, followed by subsequent decay is associated with its precipitation distribution as well. Associated convection and corresponding 500 hPa height indicates evolution of storm by day −6 and/or day −4 with peaking by day 0. Wind distribution shows symmetrical in phase movement associated with each peaking cyclonic storm.

2.4. Sub-seasonal oscillation

As discussed in the preceding section monthly (December, January, and February) interannual variabilities in precipitation are positively correlated with the corresponding seasonal (DJF) interannual variability in precipitation, but they are not in phase with each other. January interannual variability is negatively correlated with December and February interannual variabilities (Fig. 9). Seasonal (DJF) interannual precipitation variability is positively correlated with individual monthly interannual precipitation variability (0.60 for December, 0.20 for January, and 0.65 for February: Fig. 9). December and February show a higher degree of correlation than does January. It was found, however, that monthly anomalous interannual variabilities in the winter months (December, January, and February) were negatively correlated with one another. January interannual variability was negatively correlated with interannual variability in December (−0.29) and February (−0.30).

ENSO forcing has a similar behavior during the whole season (DJF), and thus the reason that the January interannual variability is opposite of December and February is unclear. To address this question, a seasonal and monthly composite analysis for selected extreme precipitation years is deliberated to explain it further during IWM.

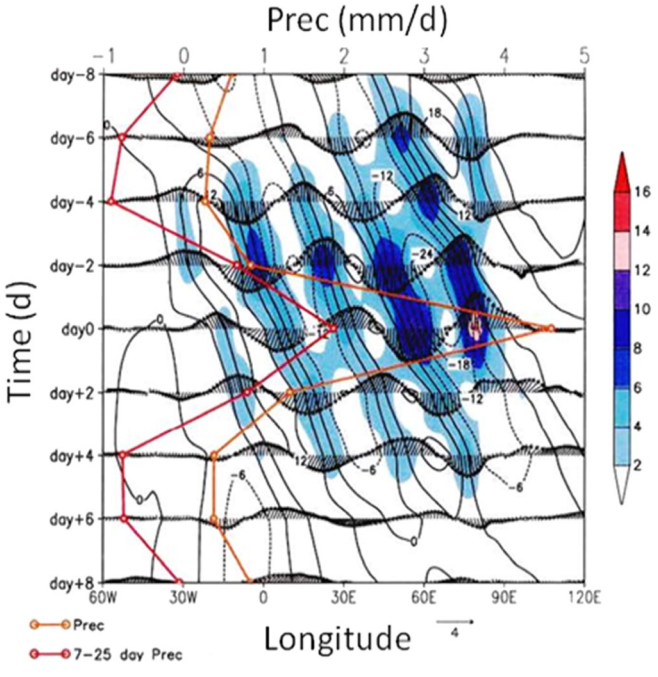

Fig. 8. Time-longitude cross-sectional distribution at 35°N of composites for 7–25-day filtered OLR (W/m^2; shade), 500-hPa height (hPa; contour), 500-hPa wind (m/s; arrow), and precipitation (mm/d; red curve; upper axis) anomalies from day −8 to day +8 based on WHDP. Day 0 corresponds to the active peak of 7–25-day WHDP variation. The yellow curve corresponds to anomalous precipitation (mm/d; yellow curve; upper axis) from day −8 to day +8 based on WHDP. (For interpretation of the references to color in this figure legend, the reader is referred to the web version of this article.)

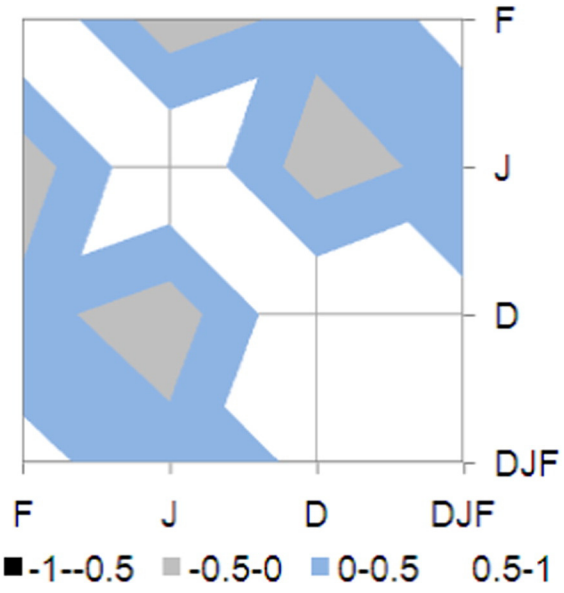

Fig. 9. Correlation between seasonal (DJF) and monthly (Dec., Jan., and Feb) interannual precipitation variability based on APHRODITE.

2.4.1. Results and discussion

In the following sections, discussion on the linkages of the IWM with global and local forcings to determine the reasons for the contrasting behavior of monthly interannual variabilities is presented.

2.4.1.1. Wet and dry winters over the WH. Initially the corresponding composite monthly anomalous precipitation distribution during wet (Fig. 10a, b, and c) and dry (Fig. 10d, e, and f) years was analyzed. To remove the effect of inadequate in situ observations from the observational reanalysis field, masking with a 10 mm/mon threshold was employed. This indicates that January anomalous precipitation is reduced (enhanced) during wet (dry) years (see Fig. 10b, e) than in December (Fig. 10a, d), and February (Fig. 10c,f). The January composite precipitation for wet (dry) years shows less (more) precipitation than the December and February values. In the case of composite precipitation for dry years, January shows a relatively higher anomalous precipitation when compared with December and February. Such contrasting sub-seasonal behavior during IWM is presented, deliberated and a rationale for such patterns and associated variability is explained.

2.4.1.2. Circulation. During extreme winter, significant anomalous cyclonic circulation associated with the IWM exists over the Himalaya due to suppressed convection over the western equatorial tropical Pacific (Kawamura, 1998; Dimri, 2013a). To assess this dynamical role during excess and deficit IWM, Fig. 11 presents wet-minus-dry composites at the 200 hPa height (contours) and wind (vector) for December (Fig. 11a), January (Fig. 11b), and February (Fig. 11c), respectively. The hatched region corresponds to a ≥95% significance level. Similarly, only wind data at the ≥95% significance level is shown. Broad differences between the wet and dry monthly composites indicate that in

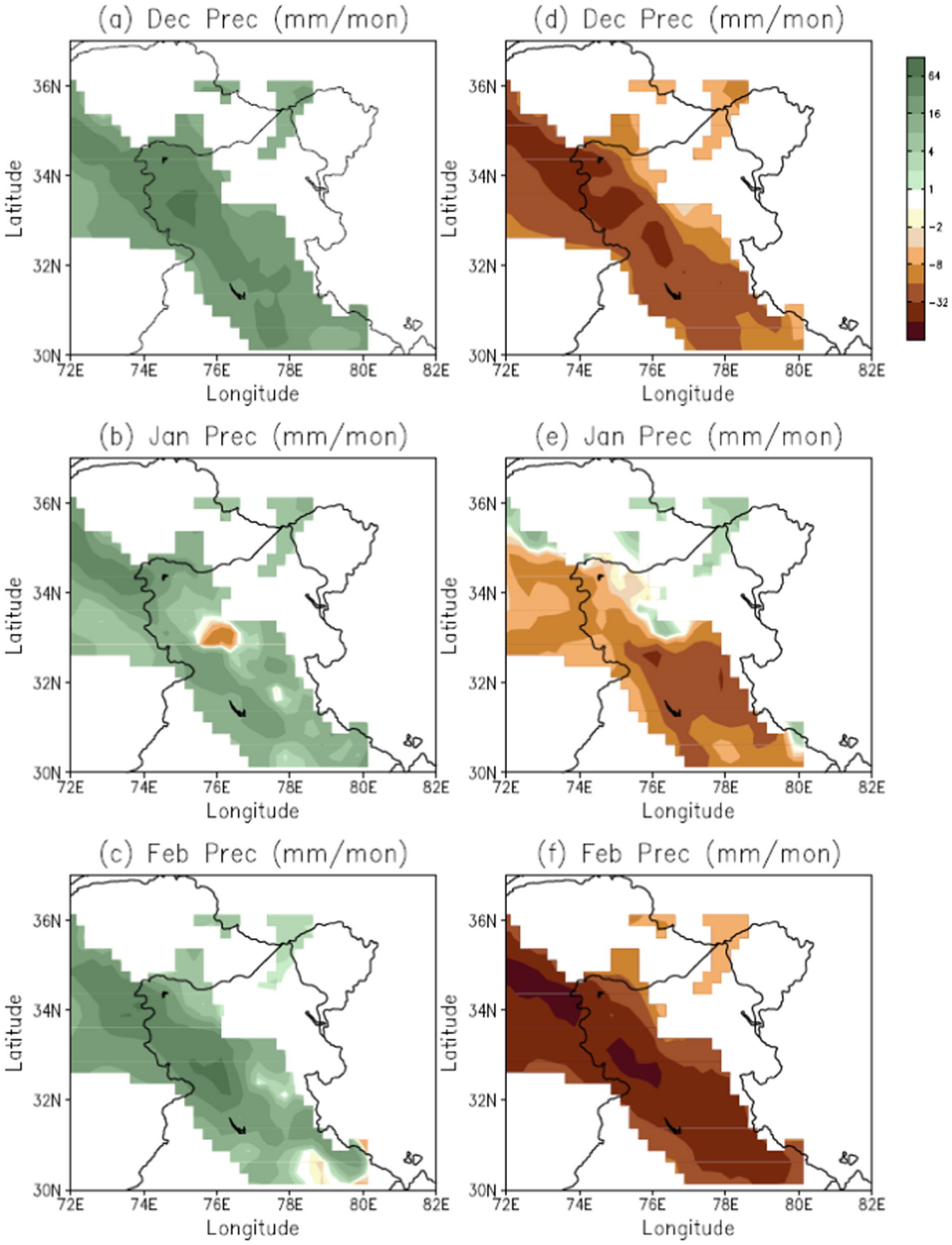

Fig. 10. Cumulative average monthly anomalous precipitation (mm/mon) during wet composites of (a) Dec., (b) Jan., and (c) Feb. and for dry composites of (d) Dec., (e) Jan., and (f) Feb. Masking with 10 mm/mon was employed.

the upper troposphere, a significant anomalous cyclonic circulation extending up to the South China Sea prevails over the Himalaya during December and February which weakens during January and is not significant. Another anomalous anticyclonic circulation located over the Siberian region during December weakens and becomes more elongated during January and shifts northward during February. During January, a well-defined anomalous anticyclonic circulation exists over the North African region to the west of the Himalaya. Corresponding wind fields suggest that over the north Himalaya/Tibetan Plateau, slower westerlies prevail during wet years. In particular, slower westerlies dominate during December and February. In the mid-troposphere, at 500 hPa, anomalous cyclonic circulation over and

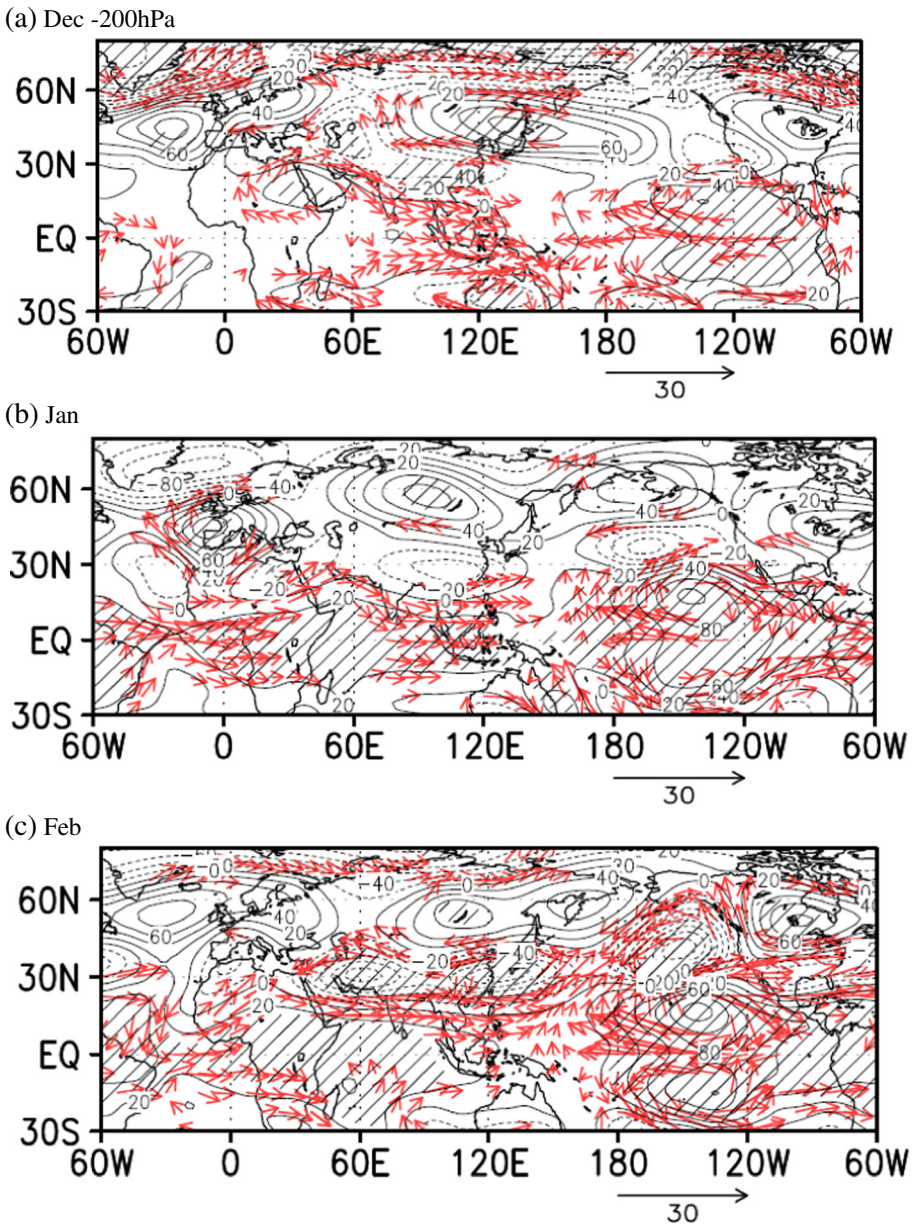

Fig. 11. Monthly difference in (wet–dry) anomaly for 200-hPa geopotential height (hPa, contour) and wind vector (m/s, arrow) for (a) Dec., (b) Jan., and (c) Feb. The hatched region corresponds to ≥95%. Similarly, only winds with 95% significance and above are shown.

around the WH prevails during December and January (data not shown). Detailed scrutiny indicates that during December, an elongated significant anomalous cyclonic circulation spreads over the west of the Himalayan region and then decays during January. However, an anomalous anticyclonic circulation over the Caspian Sea region prevails, which strengthens during January and becomes an anomalous cyclonic circulation during February. It was observed that during January, the anomalous cyclonic circulation weakens over the Himalaya, in contrast to the situation observed during December and February. Corresponding significant wind data indicates that winds over the equatorial Indian Ocean, which are slower westerlies during December, are almost neutral during January and then become faster during February. In addition, northward propagation weakens during January. In the lower troposphere, at 850 hPa, stronger northwest wind propagation dominates during December and February becoming almost neutral during January (data not shown). This propagation at the surface, arising from moisture flux transport from the equatorial Indian Ocean to the WH, strengthens the IWM during December and February more than during January.

Corresponding air temperature condition based on upper tropospheric wet-minus-dry composite associated with the IWM illustrates the above mechanism (data not shown). It can be clearly observed that January is much warmer over the Himalaya than December and February during wet seasons. This anomalous warming during January may be due to the presence of anomalous anticyclonic circulation, which in the process reduces flux exchanges from northern winter currents. This anomalous warming during January may contribute to a weakening of cyclonic formation in the sub-seasonal phase. At the mid-tropospheric level (data not shown) January also exhibits an anomalous warming over the Himalayan region, greater than that during December and February. Similarly, in the lower troposphere, at 850 hPa (data not shown), significant cooling occurs over the head of the Arabian Sea and the entire Indian subcontinent during December and February, in contrast to the relative warming observed during January.

To analyze the associated convection on the global scale, Fig. 12 illustrates the anomalous OLR for wet-minus-dry month composites. The

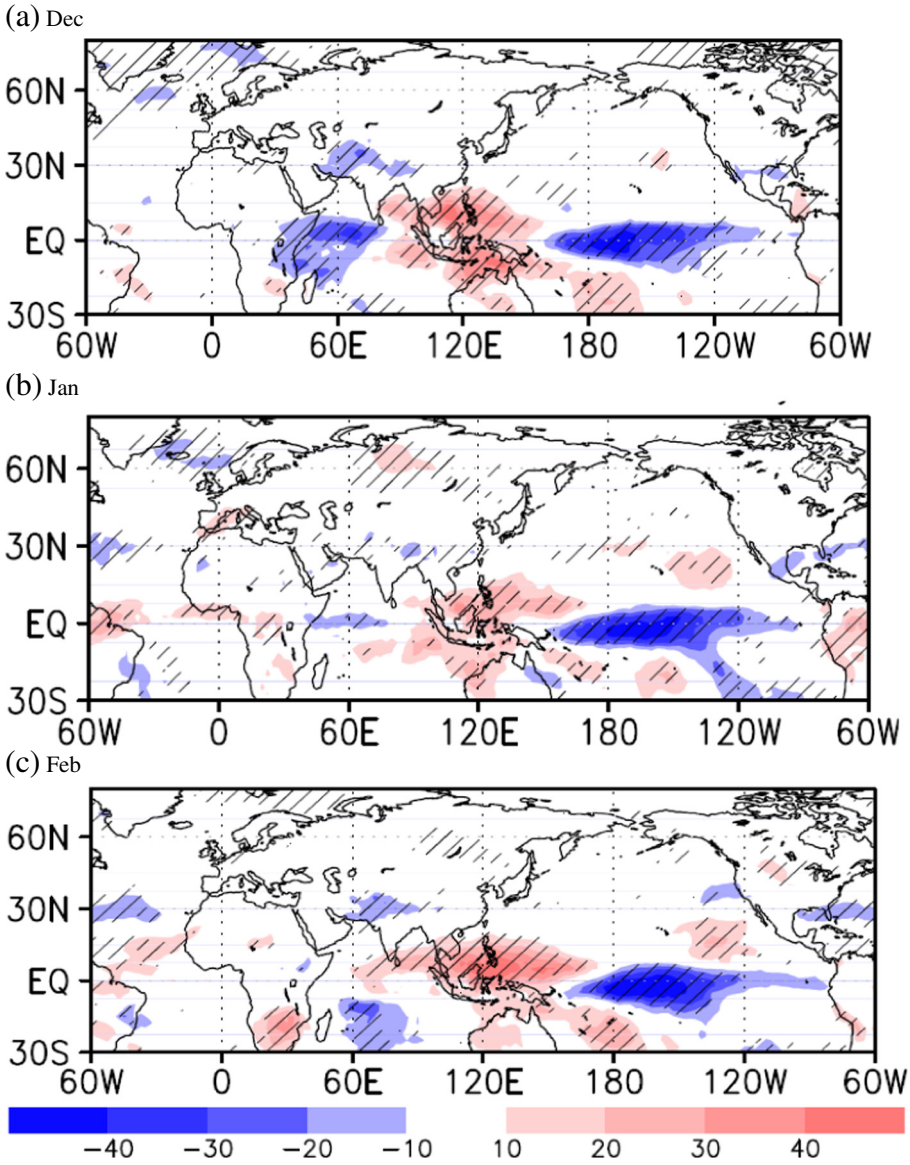

Fig. 12. Same as Fig. 11, but for outgoing longwave radiation (W/m^2, shaded).

resulting OLR distribution shows a negative OLR (strong convection) over the eastern equatorial Pacific Ocean, a positive OLR (weak convection) over the western equatorial Pacific Ocean, and a negative OLR (strong convection) over the Indian Ocean. This distribution of OLR is related to warming (cooling) of the eastern (western) equatorial Pacific Ocean linked with El Niño. During the positive phase of El Niño, enhanced warming is associated with strong convection and hence enhanced cloud cover over the eastern equatorial Pacific region, whereas suppressed convection occurs over the western equatorial Pacific region due to anomalous cooling. This suppressed convection over the western equatorial Pacific Ocean generates increased anomalous cyclonic circulation over the Himalayan region due to the Rossby response (Kawamura, 1998; Dimri, 2013a). Convection associated with attenuated Walker circulation over the eastern equatorial Pacific Ocean remains similar during all three months, but convection is suppressed over the western equatorial Pacific Ocean, and convection over the equatorial Indian Ocean weakens more during January than during December and February. The Indian Ocean exhibits higher convection during December and February, which does not occur during January. The increased convection over the Indian Ocean is mainly suppressed by low-level clouds during the IWM (Bony et al., 2000). This stronger heating during December and February compared with January (around ~60–70°E) enhances the Hadley circulation during December and February compared to January (Tanaka et al., 2004), along with an attenuated Walker circulation (Kawamura, 1998). This increased Hadley circulation provides a greater mass transport from the Southern to Northern Hemisphere during December and February when compared to January.

Corresponding monthly moisture fluxes (wet–dry) and divergence were analyzed to establish the repercussion of the dynamics discussed above (data not presented). It depicts the enhanced convergence over the WH associated with the IWM during December, which almost becomes neutral during January and then shows higher convergence during February again. Stronger anomalous southwesterly moisture fluxes transport moisture from the equatorial Indian Ocean to the Himalayan region (Dimri, 2007). During January, this flow weakens and becomes anomalously high over the Arabian Sea. To investigate this further, Fig. 13 illustrates the longitudinal–vertical cross-sectional distribution of anomalous meridional transport at 30°N during wet (Fig. 13a, b, and c) and dry (Fig. 13d, e, and f) months. It can be clearly seen that

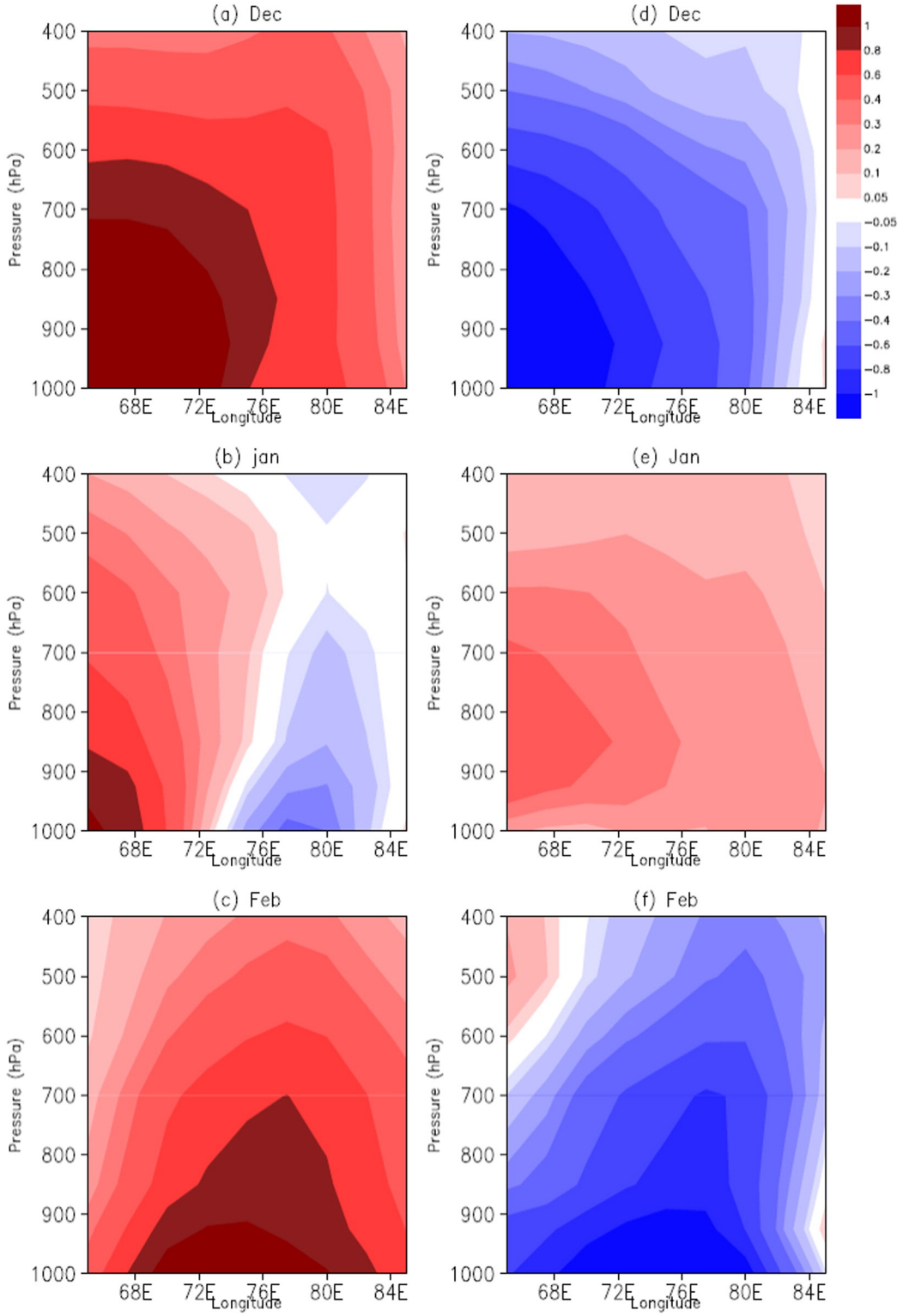

Fig. 13. Longitude–pressure vertical cross section at 30°N of the anomalous meridional moisture flux (kg/m/s) during wet ((a), (b), and (c)) and dry ((d), (e), and (f)) composites of Dec., Jan., and Feb., respectively.

wet conditions in December and February result in higher meridional moisture flux, which weakens during January particularly beyond 75°E and in the lower troposphere. During dry composites, the opposite is seen.

During an El Niño phase, symmetric circulations over the equatorial Pacific Ocean, anticyclonic in the Northern Hemisphere and cyclonic in the Southern Hemisphere, start building up in December and peak in February. The response from the IWM is similar throughout the winter. For the whole winter season (DJF), the IWM remains in phase with these when compared to January. The anomalous lower precipitation during January is influenced by sub-seasonal oscillations within the IWM. The discussion above suggests that warming/cooling of the Indian Ocean basin seems to be the dominant effect in defining sub-seasonal behavior during the IWM.

2.4.1.3. Large-scale global and local forcings. To determine large-scale global forcings, first the correlation of monthly winter precipitation over the WH with the concurrent and preceding months' sea-surface temperature (data not shown) for 28 years (1980–2007) was studied. The correlation of December and February monthly winter precipitation over the WH with the concurrent month's sea-surface temperature reveals similar patterns. Both were positively (negatively) correlated with the eastern (western) equatorial Pacific Ocean and the equatorial Indian Ocean sea-surface temperatures. This suggests that the eastern (western) equatorial Pacific Ocean warming (cooling) during December and February is in phase with the increased precipitation over the WH. For January no significant correlation exists. Rather January precipitation is negatively correlated with the equatorial Indian Ocean sea-surface temperature of the preceding December, whereas February precipitation is strongly and positively correlated with equatorial Indian and western equatorial Pacific Ocean sea-surface temperatures of December and January. These results suggest that warming (cooling) over the eastern (western) equatorial Pacific Ocean influences December and February precipitation more than January precipitation. The Indian Ocean warming also influences December and February precipitation opposite to the influence found in January. A similar analysis using 2 m surface air temperatures shows that January precipitation is influenced more by the preceding December surface air temperature (data not shown). A correlation between January precipitation and December 2 m surface temperature indicates that the preceding month's cooling over the equatorial Indian Ocean and warming over west of the WH provides conducive conditions for higher precipitation. December cooling over the north equatorial Pacific Ocean also corresponds to the higher precipitation. A similar analysis using February precipitation and January temperature data produced opposite correlations. In this case, the equatorial Indian Ocean warming and the western (eastern) equatorial Pacific Ocean cooling (warming) were positively and strongly correlated. This may be attributed to the fact that during the wet phase, January precipitation is controlled more strongly by the Indian Ocean temperature patterns, by local forcings over the WH region, or by both, and contrasts with conditions during December and February.

To further investigate the role of air temperature in controlling precipitation, anomalous air temperatures averaged over the WH region in wet and dry monthly composites are presented in Fig. 14a and b, respectively. During the wet phase, December and February temperatures show cooling (warming) in the middle (upper) troposphere. This is in contrast to January, when warming (cooling) takes place in the middle (upper) troposphere. January remains warmer (colder) in the middle (upper) troposphere than in December and February. Also, almost similar vertical temperature distributions from the surface to the mid-troposphere are seen during January. In the case of dry years, December and February remain warmer (colder) than January from the middle to upper (lower) troposphere. In wet and dry phases, both December and February show similar vertical distributions of air temperature compared with January. Such a distribution leads to the warmer mid-atmosphere during January. The WH area-averaged anomalous 2 m surface air temperatures and anomalous precipitation for wet and dry years are shown in Fig. 14c and d. These data show that if the preceding month's surface temperature increases (decreases), the succeeding month's precipitation decreases (increases). Based on such an observation, a hypothesis is proposed that the preceding month's surface

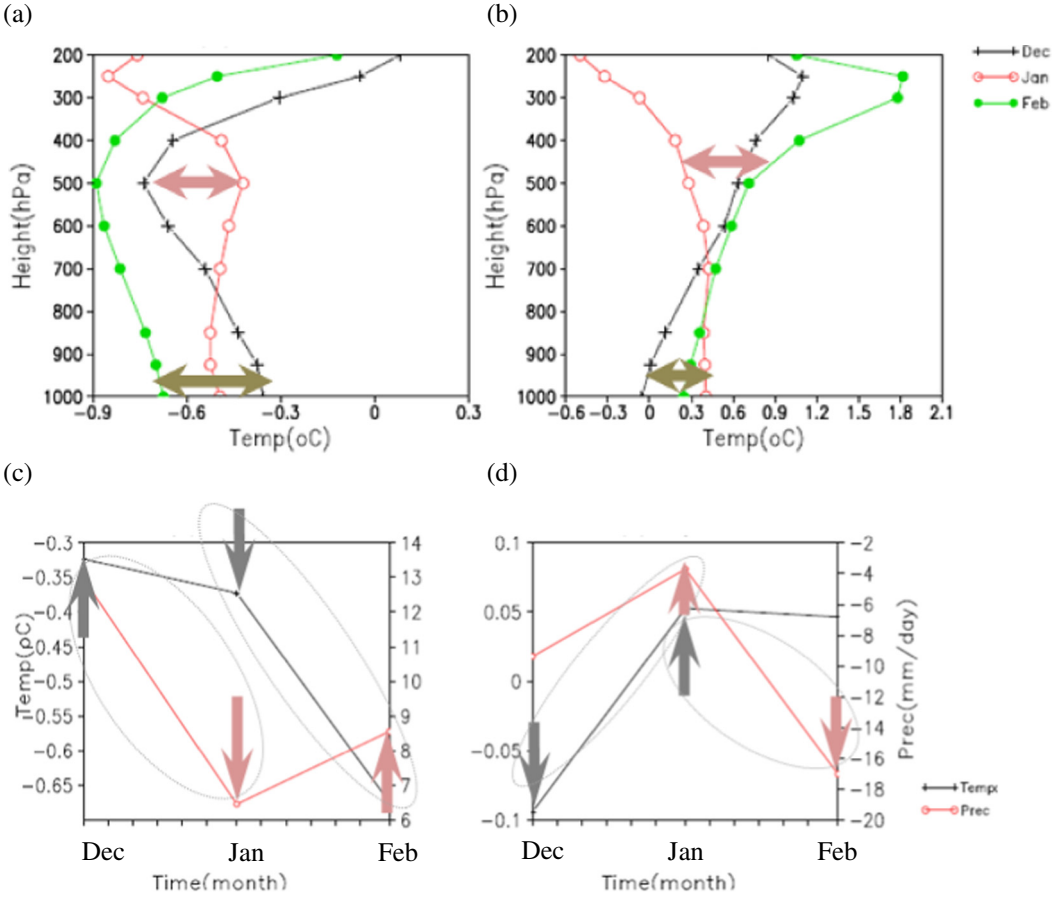

Fig. 14. Area-averaged (30°N72°E to 37°N82°E) vertical cross-sectional distribution of anomalous air temperature (°C) in (a) wet and (b) dry composites for Dec. (black line), Jan. (red line), and Feb. (green line). And area-averaged (30°N, 72°E to 37°N82°E) anomalous 2-m surface-air temperature (black line, °C) and anomalous precipitation (mm/d) during (c) wet and (d) dry year composites of Dec., Jan., and Feb. (For interpretation of the references to color in this figure legend, the reader is referred to the web version of this article.)

forcing also affects the succeeding month's precipitation. This hypothesis still needs to be studied in detail; however it is clear that subseasonal oscillations are observed in the IWM.

2.5. Interannual variability

A physical mechanism of the IWM over the WH with reference to excess/deficit years and their year-to-year variability is discussed based on the period 1980–2007 (28 years). In the following paragraphs explanations with specific reference to the sub continental and global-scale circulation changes are provided followed by deliberations on role of sea surface warming/cooling phase and associated circulation patterns in defining winter precipitation over the WH.

2.5.1. Results and discussion

Interannual variability associated with IWM over the WH is explained with a composite set of wet and dry years. Based on ±0.5 standard deviation, wet (1983, 91, 92, 95, 98, 2005) and dry (1985, 88, 97, 2000, 01, 06) precipitation years are chosen. Region from 30°N72°E to 37°N82°E (marked by the box in Fig. 1a) is selected as it receives the highest winter precipitation. Seasonal and monthly area-averaged winter precipitation anomaly is shown in Fig. 15a. There are years having excess and deficit precipitation over the region. Corresponding wet-dry composite precipitation difference with 99% confidence is depicted in Fig. 15b. It shows that significant region of higher precipitation is oriented along the WH topography which corroborates with inference of Dimri and Niyogi (2012). On global-scale circulation patterns, 200 hPa zonal wind difference between wet and dry year composites show southward movement of SWJ over and across the Indian subcontinent (Fig. 16a). In the mid latitude region, steep pressure gradient anomalies attribute to these stronger westerlies (Raman and Maliekal, 1985). At 500 hPa (Fig. 16b) significant lower geopotential right from the Saudi Arabia to the head of the Arabian Sea extending along 10°N to 30°N is seen. Weaker westerlies dominate from the Black Sea region to the northwest Indian and Tibetan Plateau region in and around 30°N. During wet years, at lower level (850 hPa, Fig. 16c) over the head of the Arabian Sea weak anomalous cyclonic surface low persists. Such mid-tropospheric circulations provide necessary convergence augmenting the precipitation mechanism by enhancing moisture supplement from the Caspian and Arabian Seas. Further, an axis of anomalous anticyclone dominates along ~60°N120°E at 200 hPa (see, Fig. 16a). Another anomalous anticyclone from the central African continent to the Indian Ocean up to Indonesia extends. A strong anomalous cyclone separates these two anomalous anticyclones and runs over the Indian subcontinent. In wet years, due to such enhanced anomalous high and low, SWJ shifts southwards. Above circulation patterns persist down in mid-troposphere as well during the wet winters (Fig. 16b). Such stronger meridional pressure gradients provide favorable conditions for frontal WDs formations. During winter, these characteristic fronts in mid-latitude westerlies generate troughs in a sequential manner which is responsible for the genesis of a number of WDs. In wet years, at 850 hPa, stronger anomalous cyclonic circulation at and around ~18°N62°E dominates (Fig. 16c). Slower westerlies around the equator and deepening of northwesterlies over the Arabian Sea exist during wet years. Such deepening brings in moisture flux over the WH during the wet years. In addition, vertical distributions of cyclonic formations immediately west of the WH create favorable conditions for higher precipitation. Anomalous velocity potential and corresponding OLR at upper troposphere are presented in Fig. 17a and b for wet and dry year composites respectively. In wet time, significant strong inflow (outflow) over the equatorial western (eastern) Pacific dominates (Fig. 17a). In dry years composite, a weak convergent source over the equatorial central Pacific exhibits (Fig. 17b). In addition, during wet years, equatorial central (western) Pacific is found to be associated with increased (decreased) convective activity. Further, lower-level increased (decreased) convection over the equatorial eastern (western) Pacific is associated with strong upward (downward) motion. In boreal winter, such situations attribute to enhanced north-south circulation in the upper tropospheric branch of the zonally symmetric Hadley circulation. Corresponding OLR distributions show strong (weak) convection followed by pronounced (reduced) cloud formation and hence reduced (enhanced) OLR over the equatorial central (western) Pacific region (Fig. 17a). A slightly decreased OLR over the WH and western Indian Ocean also corresponds to increased cloud formation. The upper tropospheric anomalous streamfunction (representing rotational part of wind) with the corresponding anomalous OLR is depicted for wet and dry year composites, Fig. 17c and d respectively. A well-defined anomalous cyclonic core is seen over the WH. In addition, an upper tropospheric low/cyclonic circulation dominates from the Mediterranean Sea to the western Pacific. El Niño formed enhanced cooling over the western equatorial tropical Pacific and hence corresponding Rossby responses (Kawamura, 1998) creates cyclonic formulations over the WH. In dry situation, anticyclonic/divergent circulation dominates over the WH (Fig. 17d).

Antecedent dependency of the IWM is as well investigated here. Lagged correlation between winter precipitation over the WH and sea surface temperature for 28 years (1980–2007) is presented in Fig. 18. IWM shows persistent and strong correlation with equatorial warming in previous seasons. Significant strong (negative) positive correlation with the eastern (western) equatorial Pacific warming (cooling) is seen right from previous winter (concurrent summer) season (Fig. 18a–e) (18c–e). This significant positive correlation with Indian

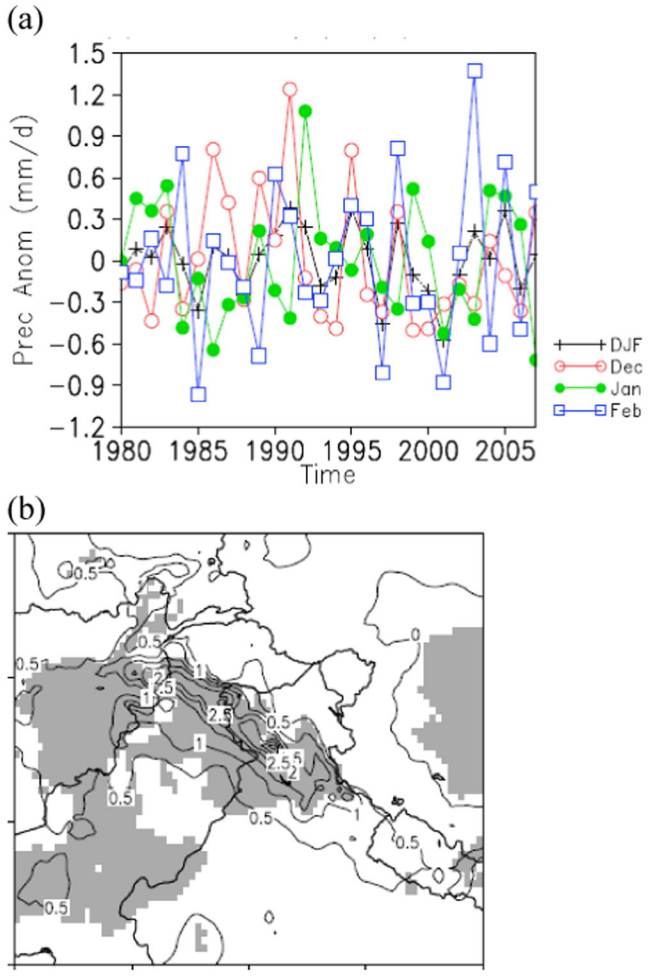

Fig. 15. (a) The monthly (Dec., Jan., and Feb.) and seasonal (DJF) precipitation (mm/d) anomaly in APHRODITE observational reanalysis and (b) difference in 3-month (Dec., Jan., and Feb.) average wet- and dry-year composites precipitation (shaded) and region with 99% confidence level (within contour).

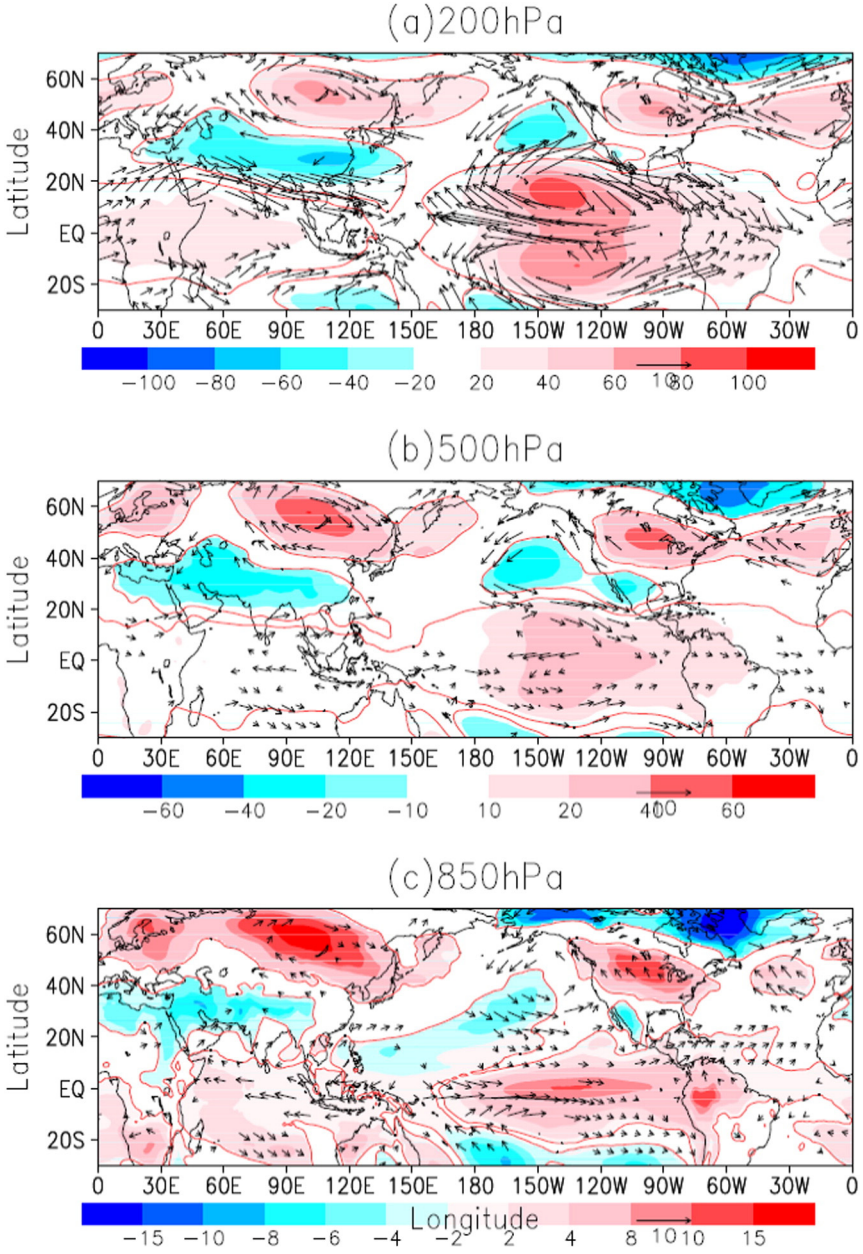

Fig. 16. Difference between 03 (DJF) month average wet and dry composites of wind (m/s: contour; winds above 99% significant level are plotted) and geopotential height (m: shaded; region within contour corresponds to 99% significant level) at (a) 200 hPa (b) 500 hPa and (c) 850 hPa.

Ocean warming increases (Fig. 18d–e) corresponding buildup of IWM by previous season (September, October, and November). By winter, equatorial eastern (western) Pacific warming (cooling) with the equatorial Indian Ocean warming corresponds to build stronger IWM. Warming over the Indian Ocean enhances northward gradient for mass transfer and hence increased response of the Hadley cell. This robustness of in tandem functioning of the enhanced Hadley cell and the attenuated Walker circulation corresponds to increased IWM which so far was not well known (Oort and Yienger, 1996; Mitas and Clement, 2005).

3. Indian winter monsoon: past

3.1. Over the Indian Himalaya

The Late Holocene climate of the Himalaya shows inverse correlation with sites solely influenced by the ISM (Fig. 19), largely because of the additional role of the WDs in the Indian Himalaya (Kotlia et al., 2012, 2015, Sanwal et al., 2013). Within the Indian Himalaya itself, even today, there are different precipitation regimes from eastern to the northwest Himalaya (Chalise and Khanal, 2001). This inverse correlation is reconfirmed by the Standardized Precipitation Index (SPI) values in Mukteshwar (Central Indian Himalaya) and Srinagar (Northwest Himalaya), the latter region is dominated by the winter rains (Fig. 20). According to the classification proposed by McKee et al. (1993), the lower SPI values reflect moderately-to-severely dry and extremely dry periods and vice versa. Therefore, the wet periods in the Central Himalaya show reverse pattern in the Northwest Himalaya (see Fig. 20) and hence the SPI provides an improved selection to develop short to long-term records for the Himalayan region which has, so far, very limited high resolution records for the Holocene period. Considering the variation in the present day climate in various sectors of the Indian Himalaya, we assume that the Holocene climate should likely be anti-correlated from east to northwest.

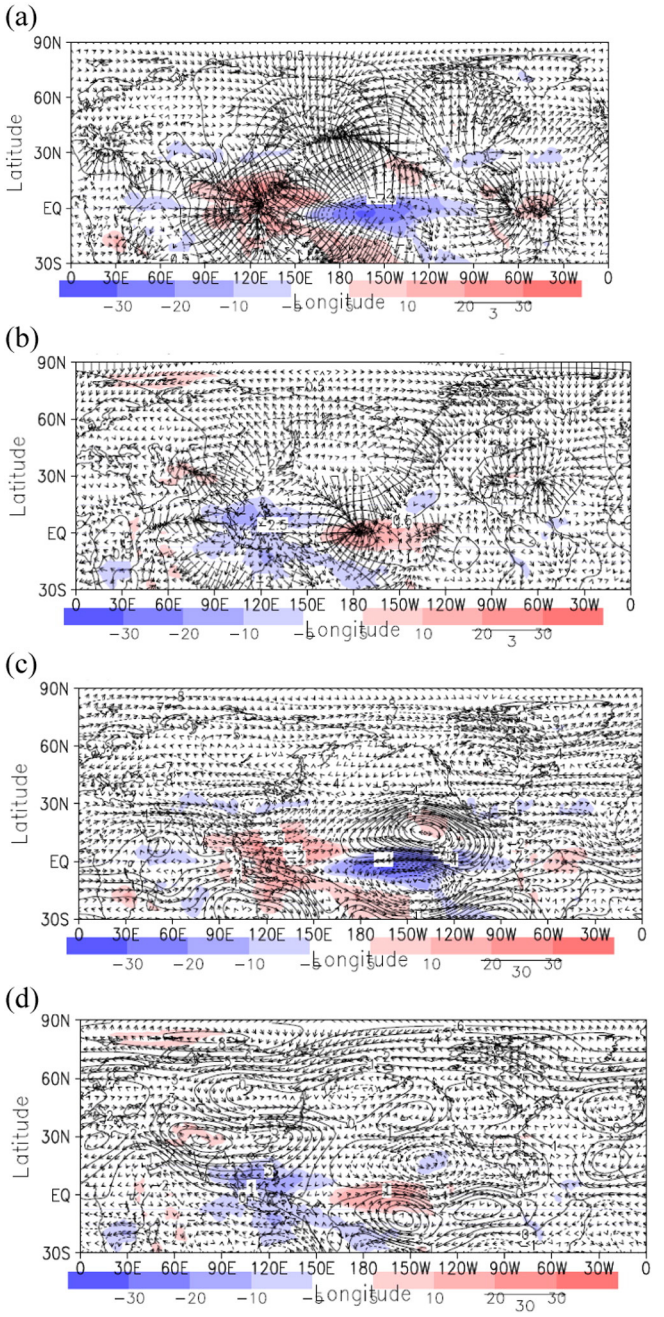

Fig. 17. Seasonal anomalous velocity potential ($*1e^{-6}$ m^2/s: contour) with corresponding anomalous divergent wind (m/s: arrow) at $\sigma = 0.1682$ and anomalous outgoing longwave radiation (W/m^2: shade) for (a) wet and (b) dry year composites. And seasonal anomalous stream function ($*1e^{-6}$ m^2/s: contour) with corresponding anomalous rotational wind (m/s: arrow) at $\sigma = 0.1682$ and anomalous outgoing longwave radiation (W/m^2: shade) for (c) wet and (d) dry year composites.

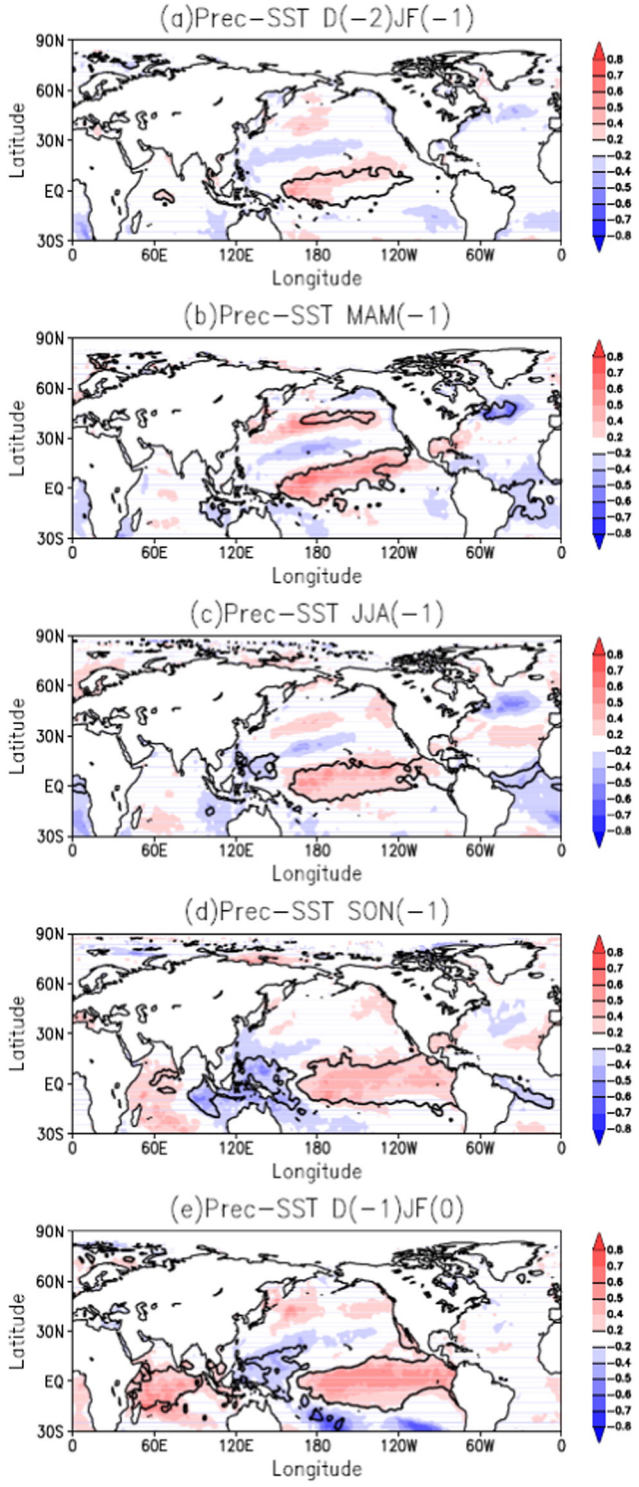

Fig. 18. Correlation between 28 years (1980–2007) area averaged winter precipitation -D(−1)JF(0) - (mm/d) with sea surface temperature (°C) during (a) D(−2)JF(−1) (b) MAM(−1) (c) JJA(−1) (d) SON(−1) and (e) D(−1)JF(0). (Figures in bracket correspond to sea surface temperature with previous and corresponding seasons). Region within contour corresponds to 99% significant level.

During the mid to late Holocene, the ISM was characterized by a decreasing strength of precipitation in concert with a southward shift of the Northern Hemisphere (NH) Intertropical Convergence Zone (ITCZ) (Gupta et al., 2003). This shift was most likely related to a decrease in the NH insolation induced by precision-paced orbital forcing. Most reports recording the Holocene ISM strength on millennial time scales are from the Indian Ocean (Anderson et al., 2002; Gupta et al., 2003) and well dated continental records from the Peninsular India (Sukumar et al., 1993; Rajagopalan et al., 1997; Yadava and Ramesh, 2001, 2005; Vishwas and Baker, 2006; Sinha et al., 2007, 2011) – the core regions of the ISM as well as nearby Oman and Socotra (Neff et al., 2001; Burns et al., 2002; Fleitmann et al., 2003, 2007; Shakun et al., 2007). In contrast, precisely dated archives near the northernmost extension of the summer ITCZ are rare (Phadtare, 2000; Rühland et al., 2006; Kotlia et al., 2000, 2010, 2015, 2016; Sanwal et al., 2013; Liang et al., 2015). However, these regions bear the potential not only to record the ISM strength but also to track the position of the boreal summer ITCZ. In the Late Holocene, important episodes were the Medieval

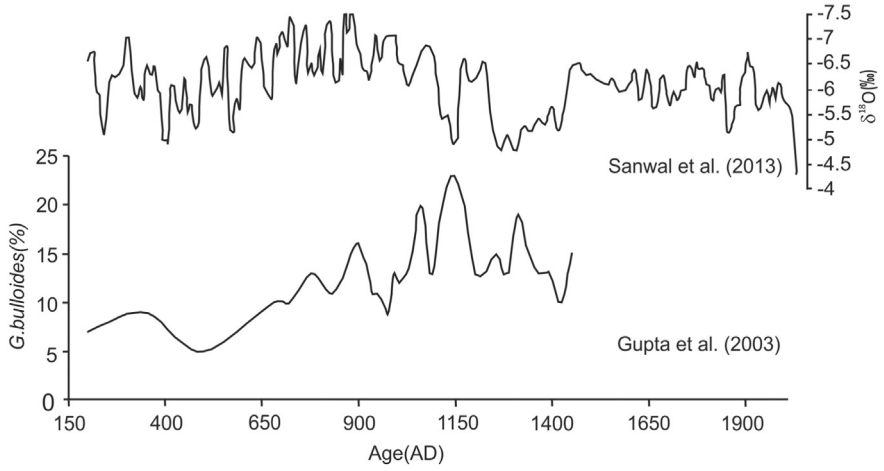

Fig. 19. Anti-correlation between Late Holocene climate of Indian Himalaya [influenced by both ISM and WDs] and Arabian Sea [dominated by the ISM]. (After Sanwal et al., 2013.)

Climate Anomaly (MCA) and LIA, which are believed to have impacted both the hemispheres but most likely not in a globally synchronous way (Grove, 1988; Kotlia et al., 2015) largely because of substantial uncertainty of the inception and duration of these episodes in different parts of the globe (Bradley, 1992; Bradley and Jones, 1993).

To understand the climate during especially the LIA, we used $\delta^{18}O$ time series data derived from two stalagmites from the Central Himalaya (Kotlia et al., 2015; Liang et al., 2015). The cave sites (Sainji and Panigarh, see Fig. 21) are situated at the northern edge of the present-day NH summer ITCZ and the stalagmites show pronounced variations in the oxygen isotope composition attributed to changes in the strength of the ISM and in the seasonality of the precipitation induced by the migration of the ITCZ.

3.2. Material and methods

Two cave carbonate stalagmites from Sainji (SA-1) and Panigarh (PGH-1), already described by Kotlia et al. (2015) and Liang et al. (2015) respectively were further interpreted for understanding the significance of the WDs in the Indian Himalaya. We used their chronology as well as $\delta^{18}O$ and $\delta^{13}C$ data for our interpretations. The central growth axis of the PGH-1 speleothem was polished and one of the exposed surfaces was scanned using a flatbed scanner at 300 dpi spatial resolution and 8 bit (256 increments) gray level (reflectance) resolution. The luminescence was measured by a digital camera fitted with filter to avoid the UV excitation energy band. Variations in gray-scale color (reflectance) and luminescence were then measured along a 10-pixel wide traverse down the central growth axis using image analysis software.

We measured the luminescence and reflectance (gray color) in the PGH-1 stalagmite. This process is based on the occurrence of organic acids in the speleothems. Generally, the plant activity is higher during wetter/warmer environment, resulting in improved quantity of organic acids (particularly humic and fulvic acids) which are trapped in the speleothem calcite. The residence times of these compounds in soils may range from decades to hundreds of years for fulvic acids and thousands of years for humic acids (Schlesinger, 1977). The humic acids are products of organic decomposition in the soil and any epikarst below it and they dissolve slowly, whereas, fulvic acids are released through plant roots and dissolved faster than humic acids (Shopov et al., 1994). The detrital content in speleothems is distinct in forms of laminations, called as luminescent bands, which are well visible through optical excitation by exposing to ultraviolet light source (Baker et al., 1993, 1998; Lauritzen and Lundberg, 1999). The color of luminescent banding, showing periodic fluctuations, is mainly due to inclusions of humic and fulvic acids, the former is darker and later is white to colorless (Gascoyne, 1977). The luminescent bands in the stalagmites, with well noticeable annual rings, can be annual and thus have been correlated with the annual precipitation and soil biotic activity (Lauritzen et al., 1986; Baker et al., 1998) and also with the solar activity. Long term changes in amplitude of the luminescence reflect shifts in both calcite growth rate and in abundance of fulvic and humic acids occluded in the growing speleothems (see Shopov et al., 1994). Generally, fulvic acids have higher luminous yields (per ppm) than humic acids, but because of higher relative concentration, they appear to be the dominant contributor to fluorescence/luminescence in the stalagmite calcite (Van Beynen et al., 2001). Under wetter/moist/warmer conditions, the bacteria break humic acids into fulvic acids which have lower molecular weight and higher content of oxygen (Liang et al., 2015) and this conversion results in stronger luminescence and higher reflectance (gray color) in the stalagmites. Therefore, luminescence and reflectance have been widely used as a proxy of the climatic change in the stalagmite research (see Baker et al., 1993; Liang et al., 2015). We measured the reflectance (gray level) and luminescence following van Beynen et al. (2001), Shopov et al., 1994 and Liang et al. (2015). In the PGH-1 stalagmite, the reflectance (0 = black; 255 = white) and luminescence (0 = black; 255 = white) values have a spatial resolution of 0.07 mm). Fig. 22 shows that the stronger luminescence together with higher reflectance point to the occurrence of colorless fulvic acids, suggesting a warmer/wetter climate, while lower luminescence (darker) coupled with darker colors indicates a cooler/drier climate (see Fig. 22).

3.3. Results and discussion

The $\delta^{18}O$ values of SA-1 cave stalagmite show a large variability between −2.1 and −8.9‰ (Fig. 23). For the late Holocene, such variations are exceptionally large and are in the order of changes as reported for glacial/interglacial transitions in the ISM domain. The exceptionally large variability in SA-1 speleothem $\delta^{18}O$ data (above 6.5‰, see Fig. 23) can be explained as below. Pausata et al. (2011) attributed a $\delta^{18}O$ variation of about 3‰ recorded in speleothems from the Himalayan foothills with precipitation difference of about 50% between warm and cold climate conditions. The SA-1 stalagmite shows even higher variations than 5‰ in their $\delta^{18}O$ values. At the same time interval, variations in $\delta^{18}O$ values as recorded in stalagmites from the monsoon core locations are considerably smaller (Fig. 23). For example, the Dongge Cave $\delta^{18}O$ time series, representing characteristics of the East Asian Monsoon (EAM) shows only a variation of <2‰ (Dykoski et al., 2005; Wang et al., 2005) and the $\delta^{18}O$ variability of a speleothem from Qunf cave, southern Oman, which identifies the strength of the ISM, is <1.5‰ (Fleitmann et al., 2007). Furthermore, stalagmites from the ISM

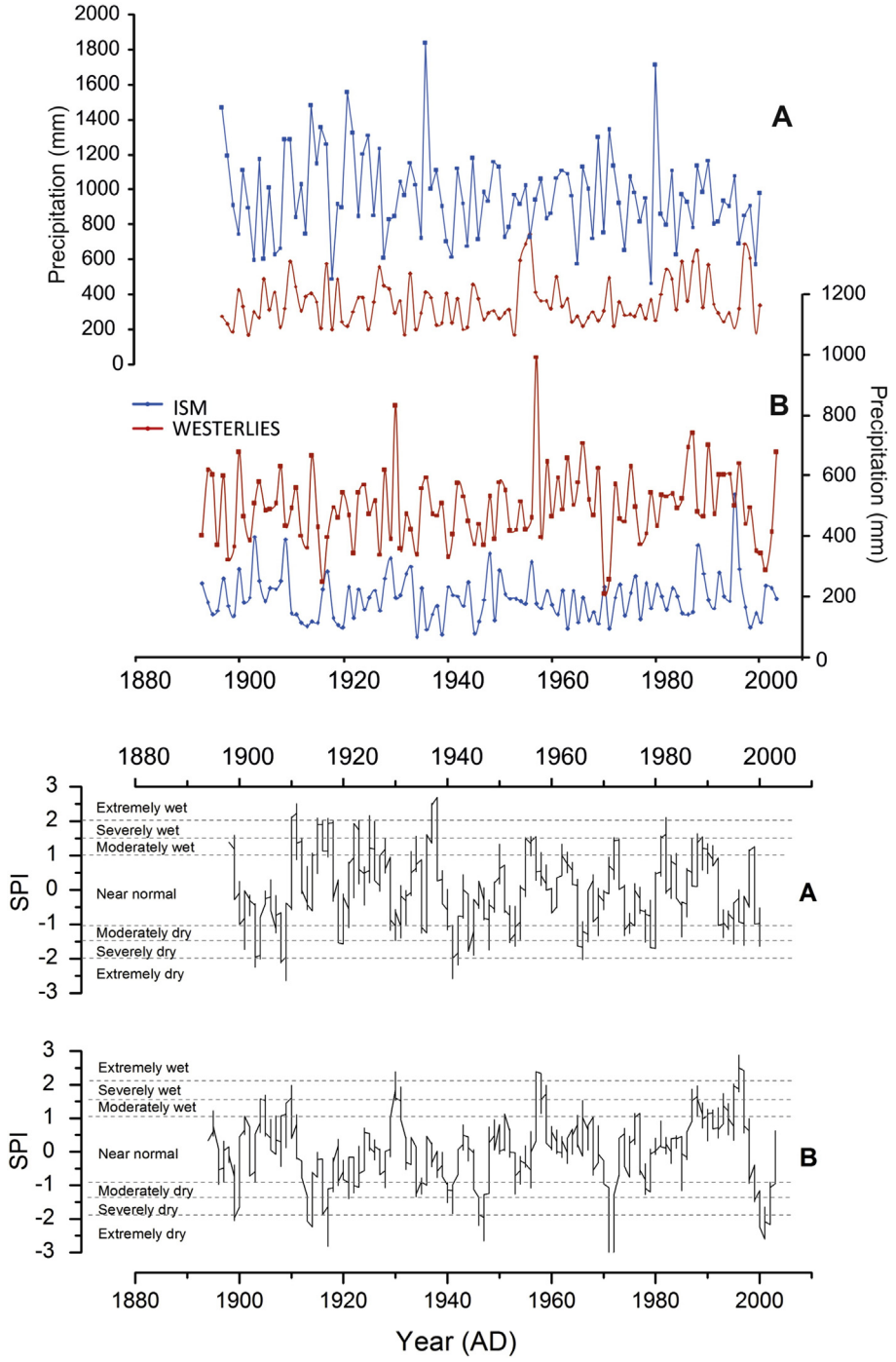

Fig. 20. Rainfall from ISM and WDs in [A] Mukteshwar [Central Indian Himalaya, 1897–2000 CE] and [B] Srinagar [Northwest Himalaya, 1893–2003 CE] and 24-month-SPI of Mukteshwar [A] and Srinagar [B]. Dry and wet rainfall intensities [near normal, moderately dry/wet, severely dry/wet, and extremely dry/wet] were defined using the SPI values following McKee et al. (1993).

core locations in Central India (Jhumar Cave, Berkelhammer et al., 2010; Sinha et al., 2011) document only changes of about 2‰ for the last 1.5 ka (see Fig. 23). In contrast to one monsoon dominated sites, the Himalayan region is sensitive to two different monsoon systems and during winter, the prevailing mid-latitude WDs provide substantial amount of rain fall. In northern India, winter precipitation is more enriched in $\delta^{18}O$ values than in summer. It is hypothesized that winter moisture might originate from recycled continental water, which then results in the observed high $\delta^{18}O$ values in precipitation (Datta et al., 1991; Araguás-Araguás et al., 1998). In other words, the ITCZ shift would not only affect the amount of precipitation in the Indian Himalayan region, it also shortens the length of the monsoon season at the cave locations (see Fig. 21), resulting in even less monsoon precipitation. At the same time, the contribution of winter precipitation to the annual mean increases. Since the WDs provide precipitation with relatively high $\delta^{18}O$ values, this would result in an additional increase in the $\delta^{18}O$ signal of the cave stalagmite, which is by far larger than observed in other speleothem studies. Decreasing $\delta^{18}O$ values, in turn, most likely characterize a northward shift of the mean latitudinal position of the boreal summer ITCZ, corresponding with a longer monsoon season and larger monsoon intensity at the caves sites. Fleitmann et al. (2007) provided a similar argumentation to explain the large $\delta^{18}O$ fluctuations

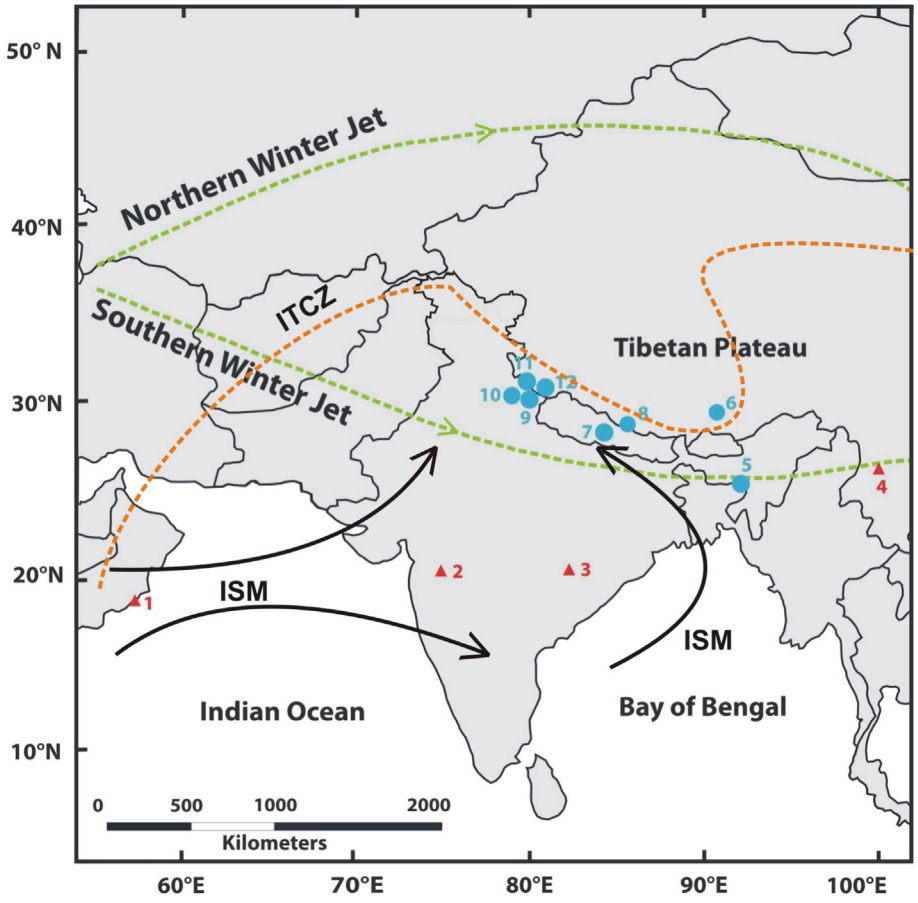

Fig. 21. Location of selected sites in the Indian subcontinent relative to the winter jet streams and position of ITCZ. Red triangles [green circles] show sites with evidence of drier [wetter] conditions during the LIA. 1] Marine core RC2735/RC2730 (Anderson et al., 2002); 2] Rivers in central and western India (Vishwas and Baker, 2006); 3] Jhumar cave (Sinha et al., 2007, 2011); 4] Lake Erhai (Chen et al., 2005); 5] Wah Shikar cave (Sinha et al., 2011); 6] Chencuo lake (Yang et al., 2004); 7] Siddha Baba cave (Denniston et al., 2000); 8] Dasuopu ice cap (Thompson et al., 2000); 9] Panigarh [PGH-1) cave (Liang et al., 2015); 10] Sainji [SA-1] cave (Kotlia et al., 2015); 11] Chulerasim cave (Kotlia et al., 2012; Duan et al., 2013); 12] Pinder valley (Rühland et al., 2006). (For interpretation of the references to color in this figure legend, the reader is referred to the web version of this article.)

(~5‰) measured in stalagmite from Hoti cave (Northern Oman) covering the last 2.5 ka. As for SA-1, higher $\delta^{18}O$ values in Hoti cave suggest that the ISM contribution to the annual precipitation decreases during weakening of the ISM in the Southern Oman.

From PGH-1 stalagmite, the multi-proxy data including oxygen and carbon stable isotopes, reflectance (gray-scale color) and luminescence point to a wetter and cooler LIA in this area. Fig. 24 presents strong evidence that the changes in climate in monsoon Asia since 1256 CE are

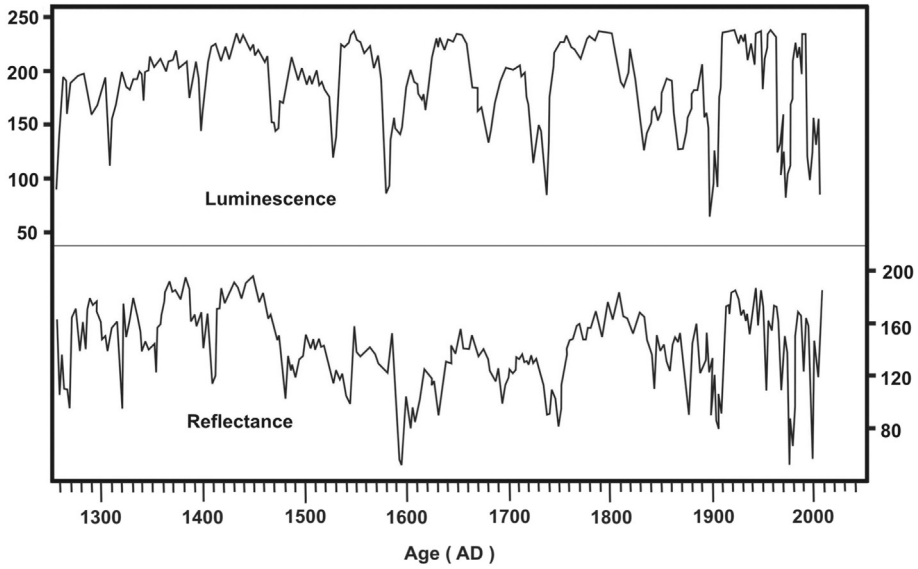

Fig. 22. Luminescence and reflectance [gray color] as climate proxies for past climatic changes: example from PGH-1 stalagmite [vertical scale, 0 = black [dark = unfavorable climate], 255 = white [lighter color = wetter/warmer climate].

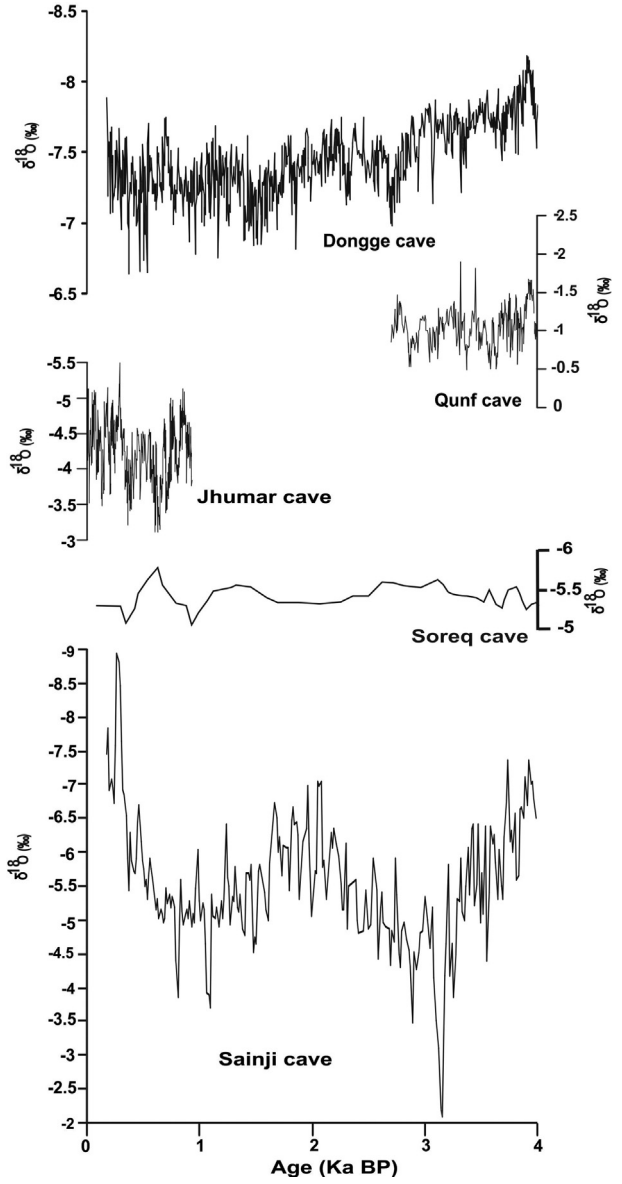

Fig. 23. $\delta^{18}O$ time series of caves influenced primarily by single monsoon from Dongge cave (Wang et al., 2005), Qunf cave (Fleitmann et al., 2007), Jhumar cave (Sinha et al., 2011) and Soreq cave (Bar-Matthews et al., 2003) and comparison with SA-1. Note the extreme variability in $\delta^{18}O$ values in SA-1 stalagmite reflecting more than one driver of monsoon in the Indian Himalaya. Dongge cave is chiefly influenced by the EAM while Jhumar and Qunf caves are within the ISM. Soreq cave is exclusively influenced by the WDs.

related to change in monsoon strength. The question is what external forces cause variations in the strength of ISM and EAM. Earlier studies have found correlations between climate and solar irradiance (e.g., Agnihotri et al., 2002) and PGH-1 records correlates strongly with variations in solar irradiance and sunspot activity (Fig. 24B and E). Periods of low solar irradiance including sunspot minima correlate with the periods of low $\delta^{18}O$ and $\delta^{13}C$ in the PGH-1 record. In particular, the Spörer and Maunder minima at ca. 1500 and 1700 CE respectively correspond with low values of $\delta^{18}O$ and $\delta^{13}C$ at approximately similar times in our record. Correlations with the Wolf and Dalton sunspot minima, centered around 1300 and 1800 CE are less clear but these periods of low solar irradiance may correlate with low values of $\delta^{18}O$ and $\delta^{13}C$ at ca. 1340 and 1760 CE. The correlation with the Spörer and Maunder minima are striking and suggest increased wetness at Panigarh during sunspot minima and low solar irradiance.

Variations in solar irradiance are believed to have determined the strength of ISM by varying the frequency of the El Niño and La Niña events over time, which produce weak and strong ISM respectively. Low (high) levels of irradiance produce more El Niños (La Niñas). During the LIA period, it appears that high frequency of El Niño events was responsible for drier conditions in the core monsoon zone but generated more monsoon "breaks" in the Himalaya. At the same time, lower solar irradiance cooled the North Atlantic and Eurasian land mass reducing the south-to-north temperature and pressure gradients that drive the ISM, increased snow cover and persistence in Eurasia which weakens the ISM and pushed more depressions to produce more winter precipitation in the Himalaya.

3.4. Solar irradiance, ENSO and NAO

The considerations above suggest that at Panigarh cave, low solar irradiance/low sunspot activity led to an increase in precipitation during the last ~750 years, but how? The link between solar irradiance and climate at Panigarh, and over broad regions of the area affected by the Asian Monsoon, appears to be determined by the relationship between solar irradiance and ENSO. Most winter precipitation, often constituting a major part of the annual precipitation especially in the northwestern Himalaya is associated with WDs. During the years of excess WDs in the Himalaya, the SST is above normal over the equatorial Indian Ocean, surface air temperature (SAT) is below normal over the east Mediterranean Sea and Himalaya, resulting in strengthening of the upper tropospheric WDs (Yadav et al., 2007). The NAO and ENSO, the two significant means of variability, affect large-scale climate over the Northern Hemisphere. The positive phase of NAO and the warm phase of ENSO have been linked with the intensification of the WD jet bringing precipitation to the Himalaya (Yadav, 2011). Syed et al. (2006) demonstrated the dominant influence of ENSO on precipitation over central southwest Asia as compared to NAO. The NAO appears to be associated with variations in surface WDs crossing the North Atlantic Ocean. During high NAO winters, the WDs are slightly stronger than in low NAO winters (Kripalani and Kulkarni, 1997). Model studies have shown that heating over the central Pacific Ocean results in the intensification of an upper tropospheric circulation system over the Caspian Sea, which intensifies the WDs passing over the region (Yadav et al., 2010). Common forcing of precipitation over the western Himalayan region and central southwest Asia is revealed by the significant positive relationship between the present reconstruction and mean annual precipitation anomalies over central southwest Asia. The relationship between the ENSO index and precipitation has also been observed over different regions of the Northern Hemisphere (Rodo et al., 1977; Price et al., 1998; Mariotti, 2007). Nevertheless, unlike ENSO, no clear periodicity has been identified in case of the NAO although there are several high and low index values in India in the last about 60 years (Hurrell, 1995).

Although the energy from the sun varies only 0.1% during the 11-year solar cycle, Meehl and Arblater (2009) have found that the stratospheric and ocean responses during solar maximum keep the equatorial eastern Pacific cooler and drier than usual, producing conditions similar to a La Niña event. They suggest that a solar maximum could potentially enhance a true La Niña event or dampen an El Niño event. It is thus possible that higher solar irradiance over longer time scales could result in La Niña conditions being favored and even enhanced over El Niño conditions. This might explain why the core monsoon area of India receives more rain during periods of high solar irradiance, which favor La Niña than during periods of low solar irradiance which favor El Niño.

Mann et al. (2005) have modeled the Niño3 index over the last millennium using solar irradiance (Niño3 (S) by employing the Zebiak–Cane model (Zebiak and Cane, 1987) of the tropical Pacific coupled ocean–atmosphere system. The Niño3 index is an average of the sea surface temperature (SST) in the region 150°W-90°W and 5°N-5°S. When the index is positive, waters are warmer than normal and when negative cooler than normal. The results show a strong negative relationship

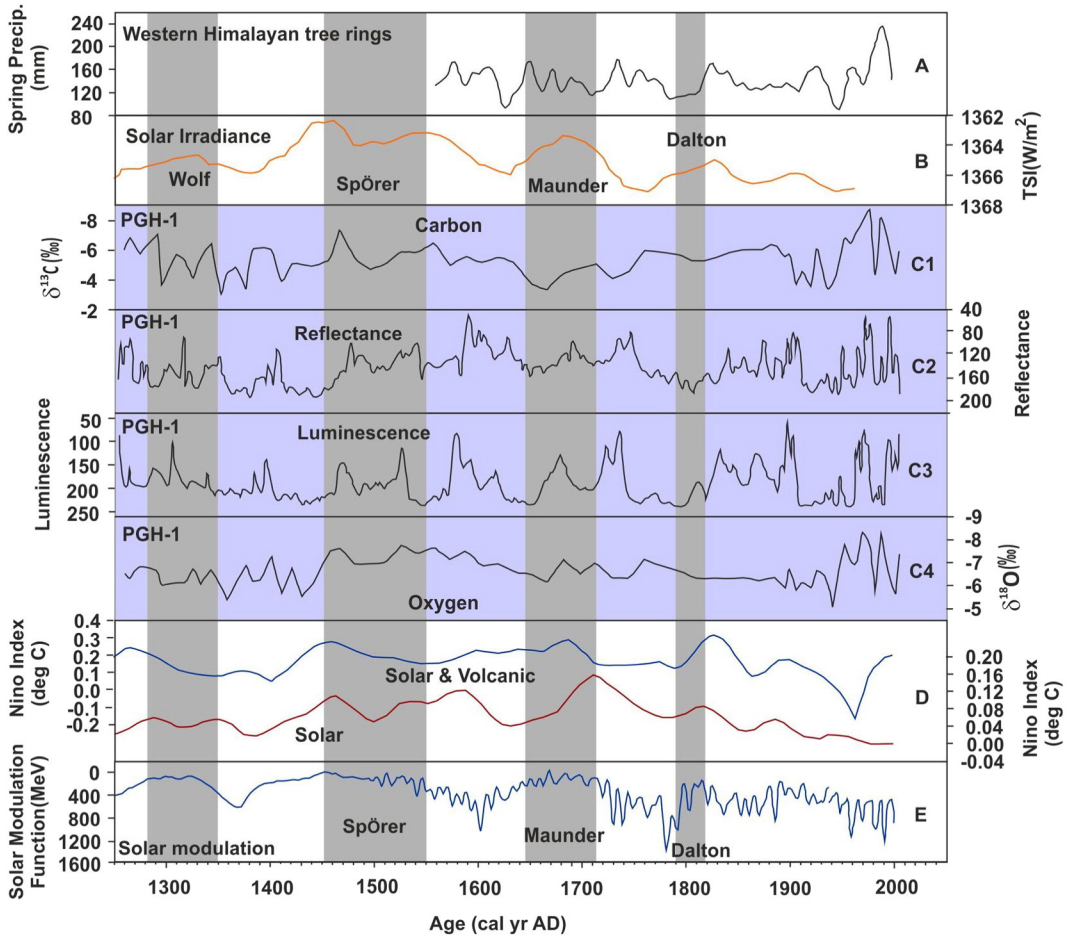

Fig. 24. Comparison of the Panigarh [PGH-1] stalagmite proxy climate record [C1-C4] with records from other sites [A] and possible climate forcings [B,D,E]. A, Tree ring precipitation record from western Himalaya data were smoothed using cubic spline designed to remove 50% of the variance with wavelength of 20 years (Singh et al., 2006); B, Solar irradiance (Bard et al., 2000); D, Nino 3.4 index (Mann et al., 2005); E, Solar modulation function (Muscheler et al., 2007).

between solar irradiance and the Niño3 index (°C), and a strong positive relationship with rainfall in Indian record. In a second modeling experiment, Mann et al. (2005) combined the impacts of volcanic and solar radiative forcing to predict Niño3 (Niño3 (S + V). Previous research has shown a statistically significant tendency towards El Niño conditions in response to past volcanic radiative forcing and in fact this modeling effort produced slightly different results (Fig. 24). Although Niño3 (S) correlates well with the India record, the Niño3 (S + V) model seems an even better predictor of climate during some time periods. This is certainly the case from CE 1000–1400, at the time of the MCA, when Niño3 indices are high ~CE 1050 while Niño3 (S + V) indices are relatively low from CE 1050–1250. The weak relationship between solar minima and $\delta^{18}O$ values can be ascribed to the "amount effect".

In fact, the strength of the ISM is closely related to ENSO conditions with weaker ISMs linked to El Niño and stronger ISMs to La Niña (e.g. Dai and Wigley, 2000; Lakshmi et al., 2003; Borgaonkar et al., 2010).This negative relationship between El Niño and rainfall is due to anomalous Walker circulation between the Indian and Pacific Oceans, resulting in anomalous regional Hadley circulation with descending motion over India and ascending motion over the equatorial Indian Ocean (Krishnamurthy and Goswami, 2000).

The solar irradiance and ENSO data in Fig. 24 support the premise that solar and volcanic radiative forcing, through its effect on ENSO, have influenced, if not controlled, rainfall in India and elsewhere in Asia since CE 1256. Variations in solar irradiance appear to have determined the frequency of ENSO warm and cold events and thus influenced the climate of India during deposition of PGH-1 from CE 1256 to CE 2005.

4. Conclusions

4.1. Indian winter monsoon: present

ISO characteristics associated with the WHDP show an average life cycle of approximately 10–12 days of evolution and decay. Dominance of ~16-day periodicity is associated with the WHDP. Correspondingly, a cascading wave train of peaking and decaying of cyclonic storm is seen. On active peak phase, convective activities in association with westerly to southwesterly enhanced moisture flux dominates and provides higher precipitation. Convection in association with the storm seems to always precede anomalous cyclonic circulation. A succession of cyclonic–anticyclonic–cyclonic, and so on, circulation dominates in the SWJ.

A physical mechanism of interannual variability associated with the IWM during wet years shows significant southward shift of the SWJ over south Asian regions. It manifests in deepening of the northwesterly incoming flow over the northern Indian region. This situation is favorable for enhanced cold surges associated with WDs. Increased convection over the central equatorial Pacific region corresponds to higher convection and hence attenuated Walker circulation. In tandem with it, strengthened Hadley Cell causing asymmetric meridional upper tropospheric flow from the Southern to Northern Hemisphere forms stationary wave in the mid-troposphere. This situation supports genesis/

intensification of WDs/troughs consisting of more frontal systems. Such situation corresponds to higher precipitation over the WH. Although the interannual variability of individual months is in phase with seasonal interannual variability, the interannual variability of individual months is not in phase with other months. A positive ENSO phase corresponds to a southward positioning/shifting of the 200 hPa SWJ. The reduction in January precipitation is influenced by the equatorial Indian Ocean surface temperature due to the weakening of the Hadley response during January compared to December and/or February. Additionally, comparatively greater middle-tropospheric warming during January enhances the middle tropospheric anticyclone with an increased northerly wind to the east compared to December and February. Such sub-seasonal/bi-monthly oscillations in the IWM correspond to higher precipitation during December and February relative to January.

4.2. Indian winter monsoon with reference to Himalaya: past

Stalagmite and other climate proxy data for the last ~4000 years suggest a broad inverse relationship between north and south India along the path of the southern winter subtropical jet, with generally increased wetness in the north and drier conditions in the south during the LIA (see Fig. 21). The available evidence implies that the pattern of wet and dry intervals seen in the PGH-1 stalagmite is a record of ENSO activity controlled by a combination of variations in solar irradiance and volcanic aerosols. This activity affected the climate of the Himalayan foothills by creating more frequent break conditions and allowing more WDs along the foothills of the Himalaya (see Kotlia et al., 2012, 2015; Sanwal et al., 2013). A higher frequency of break conditions during the LIA implies a weaker ISM that brings drier conditions to the core ISM area, but wetter conditions to northern India. If the frequency of El Niño events has varied over time, this might explain why during some periods (El Niño with more breaks), North India was wetter than the core ISM region and during others (La Niña with fewer breaks) drier than the core ISM area. In each case, conditions in the core ISM area were generally opposite those in the foothills of the Himalaya to the north.

During the LIA, the enhanced precipitation due to the WDs in the Himalaya may also have been resulted due to weakening of the ISM. A higher frequency of El Niño events would have limited transport of warm water to the North Atlantic Ocean and brought about a cooling of adjacent continents, including Europe and East/Central Asia during the LIA. This may have increased the extent of snow in northern Asia during the winter, and may even have been responsible for early snow in the region at the expanse of reduction in the ISM strength (e.g. Bamzai and Shukla, 1999; Wu and Qian, 2003; Ye et al., 2005).

The stalagmite proxy data show a broad spatial pattern in precipitation over North and South India during the LIA with northern areas showing generally increased precipitation and southern areas decreased precipitation (see Fig. 21). Since the winter and spring precipitation over the Himalaya is inversely related with precipitation in the core ISM areas (Kripalani et al., 2003), a further possible explanation for increased precipitation during LIA around Panigarh cave is that there was an increase in fall/winter/spring precipitation due to the southern winter subtropical jet depressions along the southern margin of the Tibetan Plateau.

Further, a high frequency of El Niño events during the LIA may have brought drought conditions to the core ISM area but triggered more monsoon 'breaks' that brought higher precipitation to the Himalaya. At the same time, lower solar irradiance cooled the North Atlantic and Eurasian land mass reducing the south-to-north temperature and pressure gradients that drive the ISM, increased snow cover and persistence in Eurasia, which weakens the ISM, and pushed more depressions along the path of the southern winter jet which brought more winter precipitation to the Himalaya.

We believe that changes in the dominance of El Niño and La Niña over time were a response to changes in solar forcing, namely the amount of incoming solar radiation modified by volcanic aerosols in the Earth's atmosphere, with periods of high (low) solar irradiance favoring La Niña (El Niño) conditions (Mann et al., 2005; see Fig. 24). Because lower levels of solar irradiance tend to produce El Niño conditions, these events are accompanied by less heating of the Asian continent, which is needed for a strong ISM, and by increased winter snow cover in northern Eurasia, which can also weaken the ISM. In addition, El Niño conditions reduce the flow of warm ocean water to higher northern latitudes, which cools the North Atlantic Ocean and adjacent Northern Hemisphere landmass. However, as of now, the significant influence of NAO on the WDs is not very clear except in the northwestern Himalaya (Bhutiyani et al., 2009). Therefore, based on the tree ring studies (Williams and Konovalov, 2005; Bhutiyani et al., 2009; Yadav et al., 2010, Yadav, 2011 and references therein) and speleothem research (Kotlia et al., 2012, 2016; Liang et al., 2015) in the Himalaya, we suggest that the robust climatic reconstruction from the Himalayan region by using tree ring chronology and speleothems should be useful in synoptic climatology to supplement the scarcity of instrument data from southwest Asia. For example, for better understanding of the forcing mechanism leading to increased precipitation in the Himalayan region during 1930s and 1950s when ENSO weakened considerably (Yadav, 2011), proxies like speleothems providing multi-annual to decadal scale climatic changes may supplement the existing data base.

Even though the speleothem research is growing rapidly, there are constraints in our knowledge about the sensitivity of $\delta^{18}O$ and $\delta^{13}C$ parameters. We therefore believe that long term and inter-annual cave monitoring data are required to completely understand the climate transfer functions. Secondly, the study of drip water in the caves and of modern calcite together with the careful examination of the hiatus in the sample is also important to obtain annual resolution. Thirdly, in an ideal situation, the speleothem sample displays annual layers which may be visible after it is polished. In such an ultimate situation, the speleothems can reveal annual scale climatic changes. For example, Kotlia et al. (2016) conducted such a study but found that the major difficulty in counting the annual laminae is largely due to the U/Th age errors. However, the formation of false bands or sub-annual rings needs careful approach to assume the annual scale climatic or environmental changes. Another important aspect is correlation of tree ring chronology with stalagmites from same precipitation system. Recently, Kotlia et al. (2016) observed the similar draught events in Chulerasim stalagmite as were revealed in the tree ring width chronology of the Himalayan cedar (Yadav et al., 2015)-both sites falling under the same precipitation regime. Therefore, if the above mentioned studies are carried out, speleothems can reveal more valid data on both short and long term climate variability.

However, the stalagmite research in the Himalaya has proved the significant role of the WDs in the Himalayan foothills (Kotlia et al., 2012, 2015, 2016; Sanwal et al., 2013). Also, as mentioned before, the so called global events are not synchronous throughout the globe (see Bradley, 1992; Bradley and Jones, 1993; Mayewski et al., 2004) and based on speleothem studies, we ascribe this to the different sources of the moisture, climatic variables, various precipitation patterns, geological setting of the area, composition of the host rock and trace element content in the deposited carbonate. For example, the anti-correlation between Peninsular India and Himalaya during the LIA has been regarded as additional role of the WDs in the Himalaya (Liang et al., 2015; Kotlia et al., 2016) compared to a single precipitation regime (Indian Summer Monsoon) acting in the former.

Note

As per the Indian law national boundary should be drawn. In the present study few of the figures are taken from the already published works by various researchers. Since these are old published works and

hence corresponding data and results are not archived and thus figures are kept as it is due to that limitation.

Acknowledgements

APD would like to acknowledge the use of the NCEP/NCAR reanalysis dataset from NCEP/NCAR data archive (http://www.esrl.noaa.gov/psd/data/gridded/data.ncep.reanalysis. html) for preparing the results presented in the paper. The authors also acknowledge the use of APHRODITE data (http://www.chikyu.ac.jp/precip/). Interpolated OLR data used in the study were provided by the NOAA/OAR/ESRL PSD, Boulder, Colorado, USA. We also acknowledge results from the REMO model data under EU FP7 funded HIGHNOON project (http://www.eu-highnoon.org/). BSK is thankful to the Ministry of Earth Sciences (MoES/Geosci./43/2015, New Delhi for financial support. Dr. Dallas Staley is thanked for providing English edits in the manuscript.

References

Adler, R.F., Huffman, G.J., Chang, A., Ferraro, R., Xie, P., Januaryowiak, J., Rudolf, B., Schneider, U., Curtis, S., Bolvin, D., Gruber, A., Susskind, J., Arkin, P., 2003. The version 2 Global Precipitation Climatology Project (GPCP) monthly precipitation analysis (1979-present). J. Hydrometeor. 4, 1147–1167.

Agnihotri, C.L., Singh, M.S., 1982. Satellite study of western disturbances. Mausam 33 (2), 249–254.

Agnihotri, C.L., Singh, M.S., 1987. Absorption of short-wave radiation in the atmosphere over India in winter. Mausam 38 (1), 79–84.

Agnihotri, R., Dutta, K., Bhushan, R., Somayajulu, B.L.K., 2002. Evidence of solar forcing on the Indian monsoon during the last millennium. Earth Planet. Sci. Lett. 198, 521–527.

Ananthakrishnan, R., Keshavmurty, R.N., 1973. A preliminary study of the adiabatic generation and dissipation of kinetic energy by meridional and zonal winds over India and neighborhood during winter seasons. Indian J. Meteorol. Geophys. 24, 235–244.

Anderson, D.M., Overpeck, J.T., Gupta, A.K., 2002. Increase in the Asian southwest monsoon during the past four centuries. Science 297, 596–599.

Annamalai, H., Hamilton, K., Sperber, K.R., 2007. The south Asian summer monsoon and its relationship with ENSO in IPCC AR4 simulations. J. Clim. 20, 1071–1092.

Araguás-Araguás, L., Froehlich, K., Rozanski, K., 1998. Stable isotope composition of precipitation. J. Geophys. Res. 28, 721–742.

Azadi, M., Mohanty, U.C., Madan, O.P., Padmanabhamurty, B., 2001. Prediction of precipitation associated with western disturbances using a high-resolution regional model: role of parameterisation of physical processes. Meteorol. Appl. 7, 317–326.

Azadi, M., Mohanty, U.C., Madan, O.P., 2005. Performance of a limited area model for the simulation of western disturbances. J. Aerospace Sci. Tech. 2 (2), 29–35.

Baker, A., Smart, P.L., Edwards, R.L., Richards, D.A., 1993. Annual growth banding in a cave stalagmite. Nature 304, 518–520.

Baker, A., Genty, D., Smart, P.L., 1998. High-resolution records of soil humification and paleoclimate change from variations in speleothem luminescence excitation and emission wavelengths. Geology 26, 903–906.

Bamzai, A.S., Shukla, J., 1999. Relation between Eurasian snow cover, snow depth and Indian summer monsoon: an observational study. J. Clim. 12, 3117–3132.

Bard, E., Raisbeck, G., Yiou, F., Jouzel, J., 2000. Solar irradiance during the last 1200 years based on cosmogenic nuclides. Tellus B 52 (3), 985–992.

Bar-Matthews, M., Ayalon, A., Gilmour, M., Matthews, A., Hawkesworth, C.J., 2003. Sea-land oxygen isotopic relationships from planktonic foraminifera and speleothems in the Eastern Mediterranean region and their implication for paleorainfall during interglacial intervals. Geochim. Cosmochim. Acta 67, 3181–3199.

Berkelhammer, M., Sinha, A., Mudelsee, M., Cheng, H., Edwards, R.L., Cannariato, K., 2010. Persistent multidecadal power of the Indian Summer Monsoon. Earth Planet. Sci. Lett. 290, 166–172.

Bhutiyani, M.R., Kale, V.S., Pawar, N.J., 2009. Climate change and the precipitation variations in the northeastern Himalaya: 1886-2006. Int. J. Climatol. 30, 535–548.

Bony, S., Collins, W.D., Fillmore, D.W., 2000. Indian Ocean low clouds during the winter monsoon. J. Clim. 13, 2028–2043.

Borgaonkar, H.P., Sikder, A.B., Ram, S., Pant, P.B., 2010. El Niño and related monsoon drought signals in 523-year-long ring width records of teak (Tectonagrandis L.F.) trees from South India. Palaeogeogr. Palaeoclimatol. Palaeoecol. 285, 74–84.

Bradley, R.S., 1992. When was the "Little Ice Age"? In: Mikami, T. (Ed.), Proceedings of the International Symposium on the Little Ice Age Climate. Tokyo Metropolitan University, Tokyo, pp. 1–4

Bradley, R.S., Jones, P.D., 1993. 'Little Ice Age' summer temperature variations: their nature and relevance to recent global warming trends. The Holocene 3, 367–376.

Burns, S., Fleitmann, D., Mudelsee, M., Neff, U., Matter, A., Mangini, A., 2002. A 780-year annually resolved record of Indian Ocean monsoon precipitation from a speleothem from South Oman. J. Geophys. Res. 107 (D20):4434. http://dx.doi.org/10.1029/2001JD1281.

Chalise, S.R., Khanal, N.R., 2001. An introduction to climate, hydrology and landslide hazards in the Hindu Kush-Himalayan region. In: Tianchi, L., Chalise, S.R., Upreti, B.N. (Eds.), Landslide Hazard Mitigation in the Hindu Kush-Himalaya. ICIMOD, Kathmandu, pp. 51–62.

Chen, J., Wan, G., Zhang, D.D., Chen, Z., Xu, J., Xiao, T., Huang, R., 2005. The 'Little Ice Age' recorded by sediment chemistry in Lake Erhai, Southwest China. The Holocene 15, 925–931.

Chitlangia, P.R., 1976. Mean model of western depression. Indian J. Meteor. Hydrol. Geophys. 87 (2), 157–162.

Dai, J., 1990. Climate in the Qinghai-Xizang Plateau. (in Chinese). China Meteorol. Press, Beijing.

Dai, A., Wigley, T.M.L., 2000. Global patterns of ENSO-induced precipitation. Geophys. Res. Lett. 27 (9), 1283–1286.

Das, S., 2005. Mountain weather forecasting using MM5 modelling system. Curr. Sci. 88 (6), 899–905.

Das, S., Singh, S.V., Rajagopal, E.N., Gall, R., 2003. Mesoscale modeling for mountain weather forecasting over the Himalaya. Bull. Am. Meteorol. Soc. 84 (9), 1237–1244.

Dasgupta, M., Da, S., Ashrit, R., 2012. MM5 3D-Var data assimilation and forecast system over Indian subcontinent-results from recent experiments. http://www.mmm.ucar.edu/mm5/workshop/ws04/Session5/Gupta.Das.pdf.

Dash, S.K., Chakrapani, B., 1989. Simulation of a winter circulation over India using global spectral model. Earth Planet. Sci. 98 (2), 189–205.

Datta, R.K., Gupta, M.G., 1967. Synoptic study of the formation and movements of western depressions. Indian J. Meteorol. Geophys. 18 (1), 45–50.

Datta, P.S., Tyagi, S.K., Chandrasekharan, H., 1991. Factors controlling stable isotope composition of 430 rainfall in New Delhi. India J. Hydrol. 128, 223–236.

Denniston, R.F., Gonzalez, L.A., Asmerom, Y., Sharma, R.H., Reagan, M.K., 2000. Speleothem evidence for changes in Indian summer monsoon precipitation over the last ~2300 years. Quat. Res. 53 (2), 196–202.

Dimri, A.P., 2004. Impact of horizontal model resolution and orography on the simulation of a western disturbance and its associated precipitation. Meteorol. Appl. 11, 115–127.

Dimri, A.P., 2006. Surface and upper air fields during extreme winter precipitation over the Western Himalaya. Pure Appl. Geophys. 163, 1679–1698.

Dimri, A.P., 2007. The transport of momentum, sensible heat, potential energy and moisture over the western Himalaya during the winter season. Theor. Appl. Climatol. 90 (1–2), 49–63.

Dimri, A.P., 2008. Diagnostic studies of an active western disturbance over western Himalaya. Mausam 59 (2), 227–246.

Dimri, A.P., 2013a. Interannual variability of Indian Winter Monsoon over the Western Himalaya. Glob. Planet. Chang. 106, 39–50.

Dimri, A.P., 2013b. Intraseasonal oscillation associated with Indian winter monsoon. J. Geophys. Res. - Atmos. 118 (3), 1189–1198.

Dimri, A.P., 2013c. Relationship between ENSO phases with Northwest India winter precipitation. Int. J. Climatol. 33 (8), 1917–1923.

Dimri, A.P., 2014. Sub-seasonal interannual variability associated with the excess and deficit Indian winter monsoon over the Western Himalaya. Clim. Dyn. 42 (7–8), 1793–1805.

Dimri, A.P., Mohanty, U.C., 2009. Simulation of mesoscale features associated with intense western disturbances over western Himalaya. Meteorol. Appl. 16, 289–308.

Dimri, A.P., Niyogi, D., 2012. Regional climate model application at subgrid scale on Indian winter monsoon over the western Himalaya. Int. J. Climatol. http://dx.doi.org/10.1002/joc 3584.

Dimri, A.P., Mohanty, U.C., Mandal, M., 2004. Simulation of heavy precipitation associated with an intense western disturbance over northwest Himalaya. Nat. Hazards 31 (2), 499–519.

Dimri, A.P., Yasunari, T., Wiltshire, A., Kumar, P., Mathison, C., Ridley, J., Jacob, D., 2013. Application of regional climate models to the Indian winter monsoon over the western Himalaya. Sci. Total Environ. 468. http://dx.doi.org/10.1016/j.scitotenv.2013.01.040 (iron. tion of region S36–S47).

Duan, W., Kotlia, B.S., Tan, M., 2013. Mineral composition and structure of the stalagmite laminae from Chulerasim cave, Indian Himalaya and the significance for palaeoclimatic reconstruction. Quat. Int. 298, 93–97.

Duchon, C.E., 1979. Lanczos filtering in one and two dimensions. J. Appl. Meteorol. 18, 1016–1022.

Dykoski, C., Edwards, R.L., Cheng, H., Yuan, D.X., Cai, Y.J., Zhang, M.L., Lin, Y.S., Qing, J.M., An, Z.S., Revenaugh, J., 2005. A high resolution absolute dated Holocene and deglacial Asian monsoon record from Dongge cave, China. Earth Planet. Sci. Lett. 233, 71–86.

Fleitmann, D., Burns, S.J., Mudelsee, M., Neff, U., Kramers, J., Mangini, A., Matter, A., 2003. Holocene forcing of the Indian monsoon recorded in a stalagmite from southern Oman. Science 300, 1737–1739.

Fleitmann, D., Burns, S.J., Mangini, A., Mudelsee, M., Kramers, J., Villa, I., Neff, U., Al-Subbary, A.A., Buettner, A., Hippler, D., Matter, A., 2007. Holocene ITCZ and Indian monsoon dynamics recorded in stalagmites from Oman and Yemen (Socotra). Quat. Sci. Rev. 26, 170–188.

Gascoyne, M., 1977. Trace element geochemistry of speleothems. Proc. 7th Int. Speleo. Cong., Sheffield, England, pp. 205–208.

Goswami, B.N., Mohan, R.S.A., 2001. Intraseasonal oscillations and interannual variability of the Indian summer monsoon. J. Clim. 14, 1180–1198.

Grove, J.M., 1988. The Little Ice Age. Methuen, London, p. 498.

Gupta, S.C., Mandal, G.S., 1987. Behaviour of kinetic energy generation function during a western disturbance in May 1982. Mausam 38 (1), 97–102.

Gupta, A.K., Anderson, D.M., Overpeck, J.T., 2003. Abrupt changes in the Asian southwest monsoon during the Holocene and their links to the North Atlantic Ocean. Nature 421, 354–357.

Hadley Centre, 2006. HadiSST 1.1 Global Sea-Ice Coverage and SST (1870-Present). British Atmospheric Data Centre (http://badc.nerc.ac.uk/data/hadisst).

Hara, M., Kimura, F., Yasunari, T., 2004. The generating mechanism of western disturbances over the Himalaya. 6th International GAME Conference.

Hartmann, D.L., Michelsen, M.L., 1989. Intraseasonal periodicities in Indian rainfall. J. Atmos. Sci. 46, 2838–2862.
Hatwar, H.R., Yadav, B.P., Rao, Y.V.R., 2005. Prediction of western disturbances and associated weather over Western Himalaya. Curr. Sci. 88 (6), 913–920.
Hoyos, C.D., Webster, P.J., 2007. The role of intraseasonal variability in the nature of Asian monsoon precipitation. J. Clim. 20, 4402–4424.
Hurrell, J.W., 1995. Decadal trends in North Atlantic oscillation: regional temperatures and precipitation. Science 269 (676-670).
Kalsi, S.R., Halder, S.R., 1992. Satellite observations of interaction between tropics and mid-latitudes. Mausam 43 (1), 59–64.
Kanamitsu, M., Ebisuzaki, W., Woollen, J., Yang, S.K., Hnilo, J.J., Fiorino, M., Potter, G.L., 2002. NCEP-DEO AMIP-II reanalysis (R-2). Bull. Am. Meteorol. Soc. 1631–1643.
Kawamura, R., 1998. A possible mechanism of the Asian summer monsoon-ENSO coupling. J. Meteor. Soc. Jpn. 76, 1009–1027.
Kotlia, B.S., Sharma, C., Bhalla, M.S., Rajagopalan, G., Subrahmanyam, K., Bhattacharyya, A., Valdiya, K.S., 2000. Palaeoclimatic conditions in the Late Pleistocene Wadda lake, eastern Kumaun Himalaya (India). Palaeogeogr. Palaeoclimatol. Palaeoecol. 162, 105–118.
Kotlia, B.S., Sanwal, J., Phartiyal, B., Joshi, L.M., Trivedi, A., Sharma, C., 2010. Late Quaternary climatic changes in the eastern Kumaun Himalaya, India, as deduced from multiproxy studies. Quat. Int. 213, 44–55.
Kotlia, B.S., Ahmad, S.M., Jian-Xin, Z., Raza, W., Collerson, K.D., Joshi, L.M., Sanwal, J., 2012. Climatic fluctuations during the LIA and post-LIA in the Kumaun Lesser Himalaya, India: evidence from a 400 yr. old stalagmite record. Quat. Int. 263, 129–138.
Kotlia, B.S., Singh, A.K., Joshi, L.M., Dhaila, B.S., 2015. Precipitation variability in the Indian Central Himalaya during last ca. 4000 years inferred from a speleothem record: impact of Indian Summer Monsoon (ISM) and westerlies. Quat. Int. 371, 244–254.
Kotlia, B.S., Singh, A.K., Zhao, Jian-Xin, Duan, W., Tan, M., Sharma, A.K., Raza, W., 2016. Stalagmite based high resolution precipitation variability for past four centuries in the Indian Central Himalaya: Chulerasim cave re-visited and data re-interpretation. Quat. Int. http://dx.doi.org/10.1016/j.quaint.2016.04.007.
Kripalani, R.H., Kulkarni, A., 1997. Climate impact of El Niño/La Nina on the Indian monsoon: a new perspective. Weather 52, 39–46.
Kripalani, R.H., Kumar, P., 2004. Northeast monsoon rainfall variability over south peninsular India vis-à-vis Indian Ocean dipole mode. Int. J. Clim. 24, 1267–1282.
Kripalani, R.H., Kulkarni, A., Sabade, S.S., 2003. Western Himalayan snow cover and Indian monsoon rain fall: a re-examination with INSAT and NCEP/NCAR data. Theor. Appl. Climatol. 74, 1–18.
KrishnaKumar, K., Rajagopalan, B., Cane, M.A., 1999. On the weakening relationship between the Indian monsoon and ENSO. Science 284 (5423), 2156–2159.
KrishnaKumar, K., Rajagopalan, B., Hoerling, M., Bates, G., Cane, M., 2006. Unraveling the mystery of Indian monsoon failure during El Niño. Science 314 (5796), 115–119.
Krishnamurthy, V., Goswami, B.N., 2000. Indian monsoon-ENSO relationship on interdecadal timescale. J. Clim. 13, 579–595.
Kumar, P., Rupakumar, K., Rajeevan, M., Sahai, A.K., 2007. On the recent strengthening of the relationship between ENSO and northeast monsoon rainfall over South Asia. Clim. Dyn. 28:649–660, L02706. http://dx.doi.org/10.1029/2005GL024803.
Laat, A.T.J., Lelieveld, J., 2002. Interannual variability of the Indian winter monsoon circulation and consequences for pollution levels. J. Geophys. Res. 107 (D24):4739. http://dx.doi.org/10.1029/2001JD001483.
Lakshmi Sr., S., Tiwari, R.K., Somvanshi, V.K., 2003. Prediction of Indian Rainfall Index (IRF) using the ENSO variability and sunspot cycles-an artificial neural network approach. J. Indian Geophys. Union 7 (4), 173–181.
Lang, T.J., Barros, A.P., 2004. Winter storms in central Himalaya. J. Meteorol. Soc. Jpn. 82 (3), 829–844.
Lauritzen, S.E., Lundberg, J., 1999. Speleothems and climate: a special issue of the Holocene. Holocene 9 (6), 643–647.
Lauritzen, S.E., Ford, D.C., Schwarcz, H.P., 1986. Humic substances in speleothem matrix, paleoclimate significance. Proc. 9th Int. Cong. Speleology, Barcelona, Spain, pp. 77–79.
Liang, F., Brook, G.A., Kotlia, B.S., Railsback, L.B., Hardt, B., Cheng, H., Edwards, R.L., Kandasamy, S., 2015. Panigarh cave stalagmite evidence of climate change in the Indian central Himalaya since AD 1256: monsoon breaks and winter southern jet depressions. Quat. Sci. Rev. 124, 145–161.
Liebmann, B., Smith, C.A., 1996. Description of complete (interpolated) outgoing longwave radiation dataset. Bull. Am. Meteorol. Soc. 77, 1275–1277.
Mann, M.E., Cane, M.A., Zebiak, S.E., Clement, A., 2005. Volcanic and solar forcing of the tropical Pacific over the past 1000 years. J. Clim. 18, 447–456.
Mariotti, A., 2007. How ENSO impacts precipitation in southwest central Asia. Geophys. Res. Lett. 34, L16706. http://dx.doi.org/10.1029/2007GL030078.
Mayewski, P.A., Rohling, E.E., Stager, J.C., Karlen, W., Maasch, K.A., Meeker, L.D., Meyerson, E.A., Gasse, F., Van, K.S., Holmgren, K., Lee-Thorp, J., Rosqvist, G., Rack, F., Staubwasser, M., Schneider, R.R., Steig, E.J., 2004. Holocene climate variability. Quat. Res. 62 (3), 243–255.
McKee, T.B., Doesken, N.J., Kleist, J., 1993. The relationship of drought frequency and duration to time scales. Proceedings of the 8th Conference on Applied Climatology. American Meteorological Society, Boston, MA, USA, pp. 179–183.
Meehl, G.A., Arblater, J.M., 2009. A lagged warm event-like response to peaks in solar forcing in the Pacific region. J. Clim. 22, 3647–3660.
Mitas, C.M., Clement, A., 2005. Has the Hadley cell been strengthening in recent decades? Geophys. Res. Lett. 32. http://dx.doi.org/10.1029/2004GL021765.
Mohanty, U.C., Madan, O.P., Rao, P.L.S., Raju, P.V.S., 1998. Meteorological fields associated with western disturbances in relation to glacier basins of western Himalaya during winter season. Technical Report, Centre for Atmospheric Science, IIT Delhi, India.
Mohanty, U.C., Madan, O.P., Raju, P.V.S., Bhatla, R., Rao, P.L.S., 1999. A study on certain dynamic and thermodynamic aspects associated with western disturbances over north-west Himalaya. In: Dash, S.K., Bhadur, J. (Eds.), The Himalayan Environment. New Age International Pvt. Ltd., pp. 113–122.
Mooley, D.A., 1957. The role of western disturbances in the production of weather over India during different seasons. Indian J. Meteorol. Geophys. 8 (3), 253–260.
Muscheler, R., Joos, F., Beer, J., Müller, A., Vonmoos, M., Snowball, I., 2007. Solar activity during the last 1000 yr inferred from radionuclide records. Quat. Sci. Rev. 26, 82–97.
Neff, U., Burns, S.J., Mangini, A., Mudelsee, M., Fleitmann, D., Matter, A., 2001. Strong coherence between solar variability and the monsoon in Oman between 9 and 6 kyr ago. Nature 411, 290–293.
New, M.G., Hulme, M., Jones, P.D., 2000. Representing twentieth century space time climate variability, part II: development of a 1901-96 monthly grids of terrestrial surface climate. J. Clim. 13, 2217–2238.
Oort, A.H., Yienger, J.J., 1996. Observed interannual variability in the Hadley circulation and its connection to ENSO. J. Clim. 9 (11), 2751–2767.
Pausata, F.S.R., Battisti, D.S., Nisancioglu, K.H., Bitz, C.M., 2011. Chinese stalagmite d18O controlled by changes in the Indian monsoon during a simulated Heinrich event. Nat. Geosci. 4, 474–480.
Phadtare, N.R., 2000. Sharp decrease in summer monsoon strength 4000–3500 cal years BP in the central higher Himalaya of India based on pollen evidence from alpine peat. Quat. Res. 53, 122–129.
Pisharoty, P., Desai, B.N., 1956. "Western disturbances" and Indian weather. Indian J. Meteorol. Geophys. 7, 333–338.
Price, C., Stone, L., Huppert, A., Rajagopalan, B., Alpert, P., 1998. A possible link between El Niño and precipitation in Israel. Geophys. Res. Lett. 25:3963–3966. http://dx.doi.org/10.1029/1998GL900098.
Puranik, D.M., Karekar, R.N., 2009. Western disturbances seen with AMSU-B and infrared sensors. J. Earth Syst. Sci. 118 (1), 27–39.
Rajagopalan, G., Sukumar, R., Ramesh, R., Pant, R.K., Rajagopalan, G., 1997. Late Quaternary vegetational and climatic changes from tropical peats in southern India – an extended record up to 40,000 years BP. Curr. Sci. 73, 60–63.
Raju, P.V.S., Bhatla, R., Mohanty, U.C., 2011. A study on certain aspects of kinetic energy associated with western disturbances over Northwest India. Atmósfera 24 (4), 375–384.
Rakesh, V., Singh, R., Yliya, D., Pal, P.K., Joshi, P.C., 2009. Impact of variational assimilation of MODIS thermodynamic profiles in the simulation of western disturbance. Int. J. Remote Sens. 30 (18), 4867–4887.
Raman, C.R.V., Maliekal, J.A., 1985. A northern oscillation relating northern hemispheric pressure anomalies and the Indian summer monsoon. Nature 314, 430–432.
Ramanathan, Y., Saha, K.R., 1972. Application of a primitive equation barotropic model to predict movement of "western disturbances". J. Appl. Meteorol. 11, 268–272.
Ramaswamy, C., 1966. The problem of fronts in Indian atmosphere. Indian J. Meteorol. Geophys. 17 (2), 151–170.
Rao, N.S.B., Moray, P.E., 1971. Cloud systems associated with western disturbances: a preliminary study. Ind. J. Meteorol. Geophys. 22, 413–420.
Rao, V.B., Rao, S.T., 1971. A theoretical and synoptic study of western disturbances. Pure Appl. Geophys. 90 (7), 193–208.
Rao, Y.P., Srinivasan, V., 1969. Discussion of typical synoptic weather situation: winter western disturbances and their associated features. Indian Meteorological Department: Forecasting Manual Part III.
Riehl, H., 1962. Jet streams of the atmosphere. Colorado State University, Technical Paper No. 32.
Rodo, X., Baert, E., Comin, F.A., 1977. Variations in seasonal rainfall in southern Europe during the present century: relationships with the North Atlantic Oscillation and the El Niño-Southern Oscillation. Clim. Dyn. 13, 275–284.
Roy, S.S., Bhowmik, S.K.R., 2005. Analysis of thermodynamics of the atmosphere over Northwest India during the passage of a western disturbance as revealed by model analysis field. Curr. Sci. 88 (6), 947–951.
Rudolf, B., Beck, C., Grieser, J., Schneider, U., 2005. Global Precipitation Analysis Products. Global Precipitation Climatology Centre (GPCC), DWD. Internet publication, pp. 1–8.
Rühland, K., Phadtare, N.R., Pant, R.K., Sangode, S.J., 2006. Accelerated melting of Himalayan snow and ice triggers pronounced changes in a valley peatland from northern India. Geophys. Res. Lett. 33, L15709. http://dx.doi.org/10.1029/2006GL026704.
Sanwal, J., Kotlia, B.S., Rajendran, C.P., Ahmad, S.M., Rajendran, K., 2013. Climatic variability in central Indian Himalaya during the last ca.1800 years: evidence from a high resolution speleothem record. Quat. Int. 304, 183–192.
Sato, T., Kimura, F., 2007. How does Tibetan Plateau affect transition of Indian monsoon rainfall? Mon. Weather Rev. 135, 2006–2015.
Schlesinger, W.H., 1977. Carbon balance in terrestrial detritus. Annu. Rev. Ecol. Syst. 8, 51–81.
Semwal, G., Dimri, A.P., 2012. Impact of initial and boundary conditions on simulations of western disturbances and associated precipitation. Nat. Hazards 64 (2), 1405–1424.
Semwal, G., Giri, R.K., 2007. Precipitation simulation of synoptic scale systems over western Himalayan region using Advanced Regional Prediction System (APRS) model. Mausam 58 (4), 471–480.
Shakun, J.D., Burns, S.J., Fleitmann, D., Kramers, J., Matter, A., Al-Subary, A., 2007. A high resolution, absolute-dated deglacial speleothem record of Indian Ocean climate from Socotra Island. Earth Planet. Sci. Lett. 259, 442–456.
Shopov, Y.Y., Ford, D.C., Schwarcz, H.P., 1994. Luminescent microbanding in speleothems: high-resolution chronology and paleoclimate. Geology 22, 407–410.
Singh, M.S., 1963. Upper air circulation associated with a western disturbance. Ind. J. Meteorol. Geophys. 14, 156–172.
Singh, M.S., 1971a. Study of the jet stream over India and to its north in winter: part I. Ind. J. Meteorol. Geophys. 22 (1), 1–14.
Singh, M.S., 1971b. Study of the jet stream over India and to its north in winter: part II. Ind. J. Meteorol. Geophys. 22, 149–160.

Singh, M.S., 1979. Westerly upper air troughs and development of western disturbances over India. Mausam 30 (4), 405–414.
Singh, M.S., Kumar, S., 1977. Study of western disturbance. Ind. J. Meteorol. Hydrol. Geophys. 28 (2), 233–242.
Singh, M.S., Rao, A.V.R.K., Gupta, S.C., 1981. Development and movement of a mid-tropospheric cyclone in the westerlies over India. Mausam 32 (1), 45–50.
Singh, J., Park, W.K., Yadav, R.R., 2006. Tree-ring-based hydrological records for western Himalaya, India, since A.D. 1560. Clim. Dyn. 26, 295–303.
Sinha, A., Cannariato, K.G., Stott, L.D., Cheng, H., Edwards, R.L., Yadava, M.G., Ramesh, R., Singh, I.B., 2007. A 900-year (600 to 1500 A.D.) record of the Indian summer monsoon precipitation from the core monsoon zone of India. Geophys. Res. Lett. 34, L16707. http://dx.doi.org/10.1029/2007GL030431.
Sinha, A., Stott, L., Berkelhammer, M., Cheng, H., Edwards, R.L., Budkley, B., Aldenderfer, M., Mudelsee, M., 2011. A global context for mega droughts in monsoon Asia during the past millennium. Quat. Sci. Rev. 30, 47–62.
Srinivasan, K., Ganju, A., Sharma, S.S., 2005. Usefulness of mesoscale weather forecast for avalanche forecasting. Curr. Sci. 88 (6), 921–926.
Sukumar, R., Ramesh, R., Pant, R.K., Rajagopalan, G., 1993. A d 13C record of late Quaternary climate change from tropical peats in southern India. Nature 364, 703–706.
Syed, F.S., Giorgi, F., Pal, J.S., King, M.P., 2006. Effect of remote forcing of the winter precipitation of central southwest Asia part 1: observations. Theor. Appl. Climatol. 86, 147–160.
Tanaka, H.L., Ishizaki, N., Kitoh, A., 2004. Trend and interannual variability of Walker, monsoon and Hadley circulations defined by velocity potential in the upper troposphere. Tellus 56A, 250–269.
Thomas, L., Dash, S.K., Mohanty, U.C., 2013. Influence of various land surface parameterization schemes on the simulation of the western disturbances. Meteorol. Appl. http://dx.doi.org/10.1002/met.1386.
Thompson, L.G., Yao, T., Mosley-Thompson, E., Davis, M.E., Henderson, K.A., Lin, P.N., 2000. A high-resolution millennial record of the south Asian monsoon from Himalayan ice cores. Science 289, 1916–1919.
Turner, A.G., Inness, P.M., Slingo, J.M., 2007. The effect of double CO_2 and model basic state biases on the monsoon ENSO system. I: Mean response and interannual variability. Q. J. R. Meteorol. Soc. 133, 1143–1157.
Van Beynen, P., Bourbonniere, R., Ford, D.C., Schwarcz, H.P., 2001. Causes of colour and fluorescence in speleothems. Chem. Geol. 175, 319–341.
Vishwas, K.S., Baker, V.R., 2006. An extraordinary period of low-magnitude floods coinciding with the Little Ice Age: palaeoflood evidence from central and western India. J. Geol. Soc. India 68 (3), 477–483.
Wang, Y.J., Cheng, H., Edwards, R.L., He, Y., Kong, X., An, Z., Wu, J., Kelly, M.J., Dykoski, C.A., Li, X., 2005. The Holocene Asian monsoon: links to solar changes and North Atlantic climate. Science 308, 854–857.
Williams, M.W., Konovalov, V.G., 2005. GHCN: regional data base on climate of central Asia. 1, Institute of Arctic and Alpine Research, Boulder, Colorado.
Wu, T.W., Qian, Z.A., 2003. The relation between the Tibetan winter snow and the Asian summer monsoon and rainfall: an observational investigation. J. Clim. 16 (12), 2038–2051.
Yadav, R.R., 2011. Tree ring evidence of a 20th century precipitation surge in the monsoon shadow zone of the western Himalaya. India. J. Geophys. Res. 116, D02112. http://dx.doi.org/10.1029/2010JD014647.
Yadav, R.K., 2012. Why is ENSO influencing India north-east monsoon in the recent decades? Int. J. Climatol. 32 (14):2163–2180. http://dx.doi.org/10.1002/joc.2430.
Yadav, R.K., Rupa Kumar, K., Rajeevan, M., 2007. Role of Indian Ocean sea surface temperatures in modulating northwest Indian winter precipitation variability. Theor. Appl. Climatol. 87, 73–83.
Yadav, R.K., Yoo, J.H., Kucharski, F., Abid, M.A., 2010. Why is ENSO influencing northwest India winter precipitation in recent decades? J. Climatol. 23, 1979–1993.
Yadav, R.K., Ramu, D.A., Dimri, A.P., 2013. On the relationship between ENSO patterns and winter precipitation over North and Central India. Glob. Planet. Chang. 107:50–58. http://dx.doi.org/10.1016/j.gloplacha.2013.04.006.
Yadav, R.R., Misra, K.G., Yadava, A.K., Kotlia, B.S., Misra, S., 2015. Tree-ring footprints of drought variability in last ~300 years over Kumaun Himalaya, India and its relationship with crop productivity. Quat. Sci. Rev. 117, 113–123.
Yadava, M.G., Ramesh, R., 2001. Past rainfall and trace element variations in a tropical speleothem from India. Mausam 52, 307–316.
Yadava, M.G., Ramesh, R., 2005. Monsoon reconstruction from radiocarbon dated tropical Indian speleothems. The Holocene 15 (1), 48–59.
Yang, X.D., Wang, S.M., Kamenik, C., Schmidt, R., Shen, J., Zhu, L.P., Li, S.F., 2004. Diatom assemblages and quantitative reconstruction for paleosalinity from a sediment core of Chencuo Lake, southern Tibet. Sci. China Ser. D Earth Sci. 47 (6), 522–528.
Yasunari, T., Kitoh, A., Tokioka, T., 1991. Local and remote responses to excessive snow mass over Eurasia appearing in the northern spring and summer climate. J. Meteor. Soc. Jpn. 69, 473–487.
Yatagai, A., Kamiguchi, K., Arakawa, O., Hamada, A., Yasutomi, N., Kitoh, A., 2012. APHRODITE: constructing a long-term daily gridded precipitation dataset for Asia based on a dense network of rain gauges. Bull. Am. Meteorol. Soc. 93 (9), 1401–1415.
Ye, H., Bao, Z., Feng, X., 2005. Connections of Siberian snow onset dates to the following summer's monsoon conditions over Southeast Asia. Int. J. Climatol. 25, 1567–1584.
Zebiak, S.E., Cane, M.A., 1987. A model El Niño/Southern Oscillation. Mon. Weather Rev. 115, 2262–2278.